Molecular and Cellular Neuroscience 40 (2009) 225–233

Contents lists available at ScienceDirect

Molecular and Cellular Neuroscience

journal homepage: www.elsevier.com/locate/ymcne

Periventricular notch activation and asymmetric Ngn2 and Tbr2 expression in pair-generated neocortical daughter cells

Wataru Ochiai [a,1,2], Sayaka Nakatani [a,1], Taishi Takahara [a], Masahiko Kainuma [a], Makoto Masaoka [a], Sayaka Minobe [a], Masakazu Namihira [b], Kinichi Nakashima [b], Akira Sakakibara [a], Masaharu Ogawa [c], Takaki Miyata [a,c,d,*]

[a] Department of Anatomy and Cell Biology, Nagoya University Graduate School of Medicine, 65 Tsurumai, Showa, Nagoya, Aichi 466-8550, Japan
[b] Laboratory of Molecular Neuroscience, Graduate School of Biological Sciences, Nara Institute of Science and Technology, 8916-5 Takayama, Ikoma, Nara 630-0101, Japan
[c] Laboratory for Cell Culture Development, Brain Science Institute, RIKEN, 2-1 Hirosawa, Wako, Saitama 351-0198, Japan
[d] Core Research for Evolutionary Science and Technology (CREST), Japan Science and Technology Corporation (JST), Kawaguchi, Saitama 332-0012, Japan

ARTICLE INFO

Article history:
Received 20 June 2008
Revised 16 October 2008
Accepted 21 October 2008
Available online 7 November 2008

Keywords:
Asymmetric cell division
Cortex
Neurogenin2
Tbr2
Notch
Intermediate progenitor
Slice culture
Time-lapse monitoring

ABSTRACT

To understand the cellular and molecular mechanisms regulating cytogenesis within the neocortical ventricular zone, we examined at high resolution the spatiotemporal expression patterns of Ngn2 and Tbr2. Individually DiI-labeled daughter cells were tracked from their birth in slice cultures and immunostained for Ngn2 and Tbr2. Both proteins were initially absent from daughter cells during the first 2 h. Ngn2 expression was then initiated asymmetrically in one of the daughter cells, with a bias towards the apical cell, followed by a similar pattern of expression for Tbr2, which we found to be a direct target of Ngn2. How this asymmetric Ngn2 expression is achieved is unclear, but γ-secretase inhibition at the birth of daughter cells resulted in premature Ngn2 expression, suggesting that Notch signaling in nascent daughter cells suppresses a Ngn2-Tbr2 cascade. Many of the nascent cells exhibited pin-like morphology with a short ventricular process, suggesting periventricular presentation of Notch ligands to these cells.

Introduction

Formation of the neocortex relies on the precise balance between neurogenesis and maintenance of a neural progenitor pool in the pallial primordium during embryonic development (Takahashi et al., 1996; Cai et al., 2002). The mechanism of this asymmetric daughter-cell production by the progenitor population has been extensively studied, but is still not fully understood (reviewed in Guillemot, 2007; Doe, 2008; Knoblich, 2008). It has been hypothesized that the orientation of cell division at the ventricular surface (surface division) may determine the fate of daughter cells, with divisions whose axes are perpendicular to the ventricular surface giving rise to a basal neuron and an apical progenitor cell (Chenn and McConell, 1995; Zhong et al., 1996; Sanada and Tsai, 2005). However, many independent studies indicate that the frequency of these vertical divisions is very low (Smart, 1973; Landrieu and Goffinet, 1979; Hayder et al., 2003; Kosodo et al., 2004; Konno et al., 2008), and recent cell lineage tracing studies show that neocortical daughter cells generated from horizontal divisions at the ventricular surface behave differently from one another (Konno et al., 2008; Noctor et al., 2008), suggesting that the orientation of division is not the sole determinant of asymmetry. This raises the possibility that in addition to intrinsic mechanisms that may function in dividing cells at the surface, extrinsic mechanisms involving interactions between cells within the ventricular zone (VZ) (reviewed in Harris and Holts, 1990; McConnell, 1991; Temple, 1990) may also regulate or modulate cell fate and asymmetry.

In order to elucidate the intrinsic and extrinsic mechanisms regulating the asymmetric cell output of progenitor cells, a careful analysis of the spatiotemporal expression patterns of factors controlling cell fate is needed. The bHLH transcription factor Neurogenin2 (Neurog2; also known as Ngn2) plays important roles in neuronal differentiation of neocortical cells (Nieto et al., 2001; Shuurmans et al., 2004; Shimojo et al., 2008) and migration of cells from the VZ to the subventricular zone (SVZ) (Miyata et al., 2004; Hand et al., 2005; Ge et al., 2006; Nguyen et al., 2006). Some VZ-to-SVZ migrating cells directly go on to become neurons (Noctor et al., 2001, 2004; Ochiai et

* Corresponding author. Department of Anatomy and Cell Biology, Nagoya University Graduate School of Medicine, 65 Tsurumai, Showa, Nagoya, Aichi 466-8550, Japan. Fax: +81 52 744 2041.
E-mail address: tmiyata@med.nagoya-u.ac.jp (T. Miyata).
[1] These authors contributed equally to this work.
[2] Present address: Laboratory for Neocortical Development, Center for Developmental Biology, RIKEN, 2-2-3 Minatojima-Minami, Chuo, Kobe 650-0047, Japan.

1044-7431/$ – see front matter © 2008 Elsevier Inc. All rights reserved.
doi:10.1016/j.mcn.2008.10.007

al., 2007), while intermediate or basal progenitors undergo division within the SVZ to give rise to neuron pairs (Haubensak et al., 2004; Miyata et al., 2004; Noctor et al., 2004, 2008). Tbr2 (T-brain-2, also known as Eomesodermin [Eomes]) is similarly thought to be involved in differentiation of cells along the neuronal lineage, based on its expression pattern in the VZ and SVZ (Englund et al., 2005; Noctor et al., 2008). Indeed, loss of Tbr2 function in mice results in aberrant specification of intermediate progenitors and neuronal differentiation (Arnold et al., 2008; Sessa et al., 2008). Moreover, a type of human neocortical malformation is caused by mutations in this gene (Baala et al., 2007).

In spite of its well-known role in maintaining the undifferentiated state in telencephalic progenitor cells (reviewed in Gaiano and Fishell, 2002; Kageyama et al., 2005), Notch activation has not been extensively examined at high spatiotemporal resolution. Previous immunohistochemical analysis using an anti-Notch intracellular domain (anti-NICD) (Tokunaga et al., 2004) or anti-Hes1 (Shimojo et al., 2008) antibody demonstrated that nuclei with strong Notch activation are located in the upper half of the mouse neocortical VZ, away from the ventricular surface. In the retina of the developing zebrafish and chick, however, Notch is suggested to be active near the ventricle (Murciano et al., 2002; Del Bene et al., 2008). It is therefore important to carefully examine the timing and location of Notch activation relative to the morphology of VZ cells, including nascent daughter cells generated at the neocortical ventricular surface.

To track the developmental time course of Ngn2 and Tbr2 expressions in VZ cells, time-lapse observation was performed on daughter cells of individually DiI-labeled progenitor cells in cultured neocortical slices, followed by immunostaining for Ngn2 or Tbr2. We found that Ngn2 protein expression was initiated asymmetrically in the surface-generated daughter cells as early as 2 h after birth, about 2 h earlier than the onset of Tbr2 expression. Luciferase and ChIP assays further revealed that Tbr2 is directly downstream of Ngn2. Daughter cells expressing Ngn2 or Tbr2 were connected to the ventricular surface and maintained expression of the two transcription factors after detaching from the ventricular surface. Inhibition of Notch signaling in nascent surface-born daughter cells by treatment with a γ-seceretase inhibitor strikingly increased the frequency of Ngn2 expression in daughter cells 2 h after birth. Activation of Notch was observed not only in the basal VZ, but also in the periventricular VZ containing nascent daughter cells. These results suggest that the periventricular area and the initial morphology of surface-born daughter cells may be important for the regulation of cell fate choice.

Results

Behavioral asymmetry in a single clone generated at the ventricular surface

We first examined the morphological changes of daughter cells generated at the ventricular surface. Fig. 1A (also Supplemental movies 1 and 2) shows an example of asymmetric division in which one daughter cell generated at the ventricular surface of the E14 cerebral wall slice moved to the SVZ and gave rise to a pair of neurons (Hu^+, data not shown), while its sister cell divided at the ventricular surface (referred to as "asymmetric P/P division"). This pattern of asymmetric P/P division is common in cerebral walls about 200 μm thick and produces a pin-shaped daughter cell that lacks a radial (pial) process and moves to the SVZ (Miyata et al., 2004). Consistent with previous observations (Konno et al., 2008; Miyata et al., 2001, 2004; Nishizawa et al., 2007; Noctor et al., 2004, 2008; Ochiai et al., 2007), both the daughter cell that underwent the surface division and the cell that eventually moved to the SVZ were initially connected to the ventricular surface.

Timeline of Ngn2 and Tbr2 expressions in surface-born daughter cells

Since the SVZ-directed behavior we observed (Fig. 1A) suggests a cell fate bias towards the neuronal lineage, we carefully analyzed the timing of expression of the neurogenic transcription factors Ngn2 and Tbr2. Ngn2 and Tbr2 showed partially overlapping expression patterns in the VZ and SVZ of frozen sectioned cerebral walls (Figs. 1D, E), with very little signal detected at the ventricular surface. To determine whether Ngn2 and Tbr2 proteins are expressed in SVZ-directed daughter cells, live observation of individually DiI-labeled, pin-like cells at the ventricular surface was followed by immunostaining for Ngn2 or Tbr2. Ngn2 immunoreactivity was observed in cells both before (n=6/10, Fig. S1A, B) and after departure from the ventricular surface (n=3/3, Fig. S1C). Similarly, Tbr2 was detected both before (n=1/5, Fig. S1D) and after (n=2/2, Figs. 1C, S1E) departure.

To determine the onset of expression for these two factors, we immunostained daughter cell pairs whose ages were defined by live imaging from their time of birth (i.e. division of their progenitor cells) at the ventricular surface (Figs. 2A–H), a method previously established for dissociated cells (Kawaguchi et al., 2004). Each DiI^+ clone was immunostained with anti-Ngn2 or anti-Tbr2 antibody. By repeating this procedure at different time points following daughter cell birth, histograms showing the temporal expression profiles for Ngn2 and Tbr2 proteins were obtained with a time resolution of 1 h (Fig. 2I). We found that neither Ngn2 nor Tbr2 was expressed in daughter cells immediately after birth, but Ngn2 expression began about 2 h later and Tbr2 expression followed at the 4-h time point. Both factors reached an expression plateau at about 50% of total cells examined. The average distance of nuclei showing the earliest Ngn2 immunoreactivity (2 and 3 h-old daughter cells, n=6) from the ventricular surface was 20±3 μm, while that of the earliest detected $Tbr2^+$ nuclei (4 and 5 h-old daughter cells, n=5) was 28±9 μm, consistent with the *in vivo* data (Figs. 1D, E).

Tbr2 is a direct target of Ngn2

Based on the sequential onset of Ngn2 and Tbr2 expressions (Fig. 2I) and a previous report that Tbr2 is downregulated upon loss of Ngn (Shuurmans et al., 2004), we carried out a series of experiments to determine whether Tbr2 is directly downstream of Ngn2. Electroporation of the Ngn2 cDNA into the ganglionic eminence (GE), where both Ngn2 and Tbr2 are normally absent, resulted in ectopic expression of Tbr2 protein in 8.9% of transfected cells (n=1340) (Figs. 3A, B), while no $Tbr2^+$ cells were observed in control experiments (n=454 cells). Next, we performed luciferase assays using the Tbr2 promoter region (Ueno et al., 2000), which contains twelve E-boxes (Fig. S2A). Forced expression of Ngn2 in the GE resulted in activation of the Tbr2 promoter, an effect that was inhibited by coexpression of Hes1 (Fig. 3C). Similar experiments with the pallial region also resulted in activation of the Tbr2 promoter (Fig. S2B). Finally, a chromatin immunoprecipitation (ChIP) assay demonstrated that Ngn2 binds directly to the E-boxes of the Tbr2 promoter (Fig. 3D). Taken together, these results indicate that Ngn2 acts directly upstream of Tbr2.

Expression of Ngn2 and Tbr2 within clones is asymmetric and biased towards the apical cell

The plateau of Ngn2 and Tbr2 expressions at about 50% of the total number of cells examined (Fig. 2I) indicates an asymmetry in the daughter cell expression of these transcription factors. This populational asymmetry could be due to a mixed population of progenitors producing either pure Ngn2/Tbr2-positive (+/+) or negative clones (−/−) or a homogenous population of progenitors, each of which produces one positive and one negative cell (+/−). To determine which mode of division is preferred in these cells, the composition of clones containing $Ngn2^+$ (>3 h-old clones, n=29) and

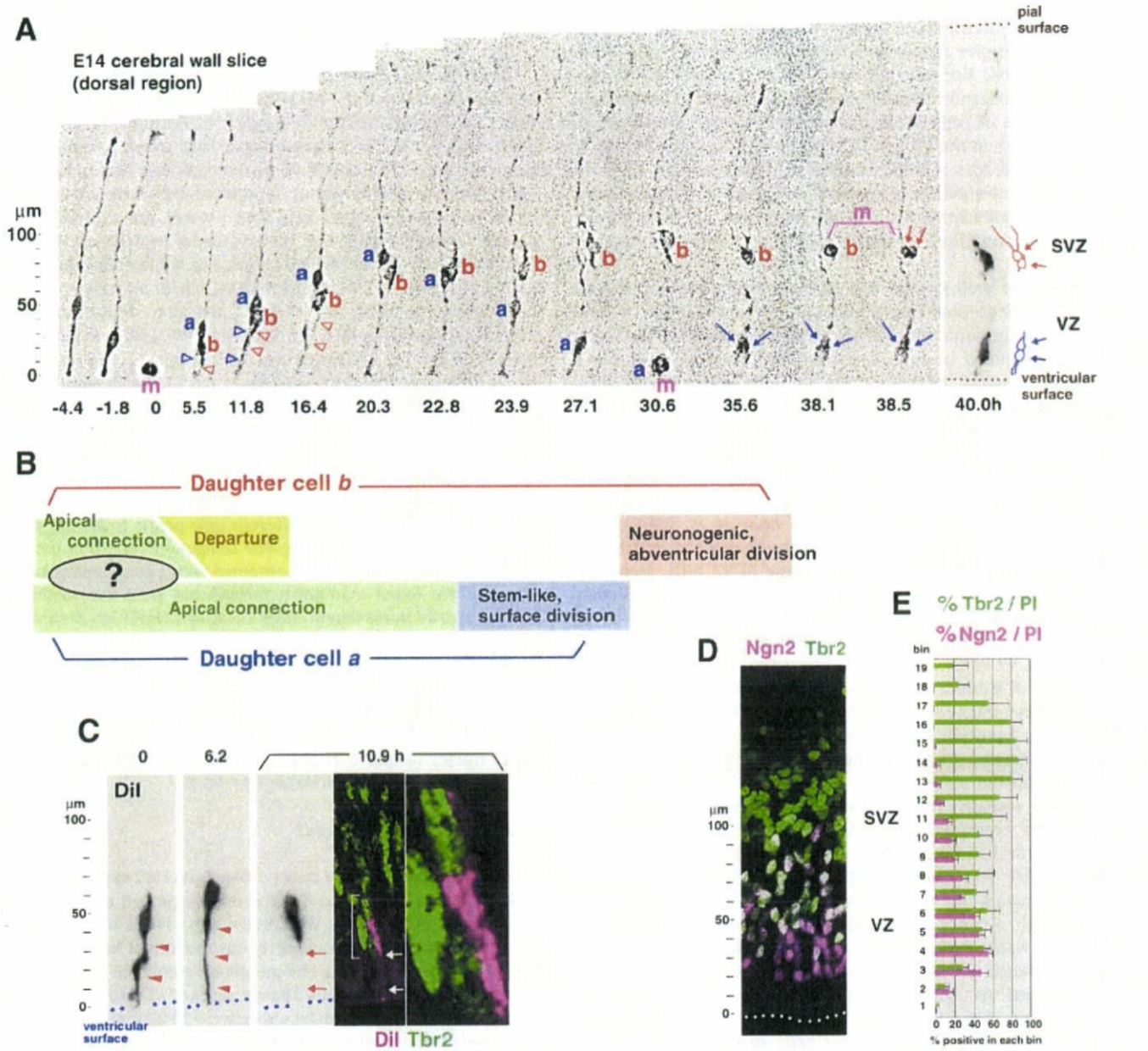

Fig. 1. Behavior and Ngn2 and Tbr2 expressions of neurogenic, intermediate cortical progenitor cells. (A) Formation of a two-cell clone from a single DiI-labeled progenitor cell in an E14 mouse cerebral wall slice. Time before mitosis (*m*) of the founder progenitor cell (−4.4 to −1.8 h), as well as elapsed time from mitosis (0–40.0 h), are indicated. Stills from live observation are all deconvoluted images taken from Supplemental movies, and the last picture (40.0 h) was taken after fixation and vibratome sectioning of the observed slice. Of the two daughter cells (*a* and *b*) generated at the ventricular surface, cell *a* inherited the pial process. Initially, both daughter cells had a ventricular process (open arrowhead). Cell *b* retracted its ventricular process by 20.3 h, moved to the SVZ, then divided abventricularly (*m*, 38.1–38.5 h). Granddaughter cells generated from this abventricular division (red arrows) were both positive for the neuronal marker Hu (Fig. S1) at 40.0 h (time of fixation). In contrast, daughter cell *a*, which is similar in shape to its parent cell (though more elongated to compensate for cerebral wall thickening), retained its ventricular process and exhibited nuclear/somal migration to the ventricular surface, where it subsequently divided (*m*, 30.6 h). This asymmetric P/P pattern of division that sends one mitotic daughter cell to the SVZ is typical in midembryonic mouse cerebral walls around 200 μm thick (Miyata et al., 2004). (B) Schematic diagram showing the distinct developmental trajectories of two daughter cells within a single clone. The question mark indicates the choice point at which one daughter cell is destined for movement to the SVZ. (C) Tbr2 immunoreactivity detected in a VZ cell retracting a ventricular process. A pin-like cell whose ventricular process was initially thick (0–6.2 h) but later collapsed, and whose soma moved adventricularly (10.9 h), a behavior characteristic of cells about to migrate to the SVZ (Miyata et al., 2004; Ochiai et al., 2007; see also Fig. S1E for a cell that has completely retracted its ventricular process). This "de-epithelialized" cell was Tbr2$^+$ at 10.9 h. (D) An E14 mouse cerebral wall section double immunostained with anti-Ngn2 (magenta) and anti-Tbr2 (green) antibody. Note the presence of double positive cells (white). Around 67% of total Ngn2$^+$ cells counted (n=275) were Tbr2$^+$, while about 40% of the total Tbr2$^+$ cells counted (n=454) were Ngn2$^+$. (E) Histogram summarizing results of Ngn2 or Tbr2 immunostaining coupled with propidium iodide (PI) staining. The proportion of the total nuclei that were positive for Ngn2 (magenta) or Tbr2 (green) was counted in each of the bins (10 μm increments from the ventricular surface). Scaling along the ventricular-pial axis is common in D and E.

Tbr2$^+$ cells (all clones, n=24) was evaluated (Fig. 2J). The majority of the examined clones were found to be +/− (66% for Ngn2 and 88% for Tbr2). The spatial relationship between the positive and negative cells in each of the +/− clones (n=19 for Ngn2 and n=22 for Tbr2) was further analyzed. The daughter cell whose nucleus was closer to the ventricular surface (the "apical daughter") more frequently expressed these transcription factors (74% for Ngn2 and 68% for Tbr2) than its sister cell (the "basal daughter"; 26% for Ngn2 and 32% for Tbr2) (Fig. 2K).

As shown earlier (Figs. 1A and 2D), surface-born daughter cells that did not inherit a pial process from the parent cell and thus adopted a pin-like morphology generally slower in their movement towards the pial side (abventricular movement) than bipolar (radial glial-like) daughter cells that inherited a pial process (Miyata et al., 2001; 2004).

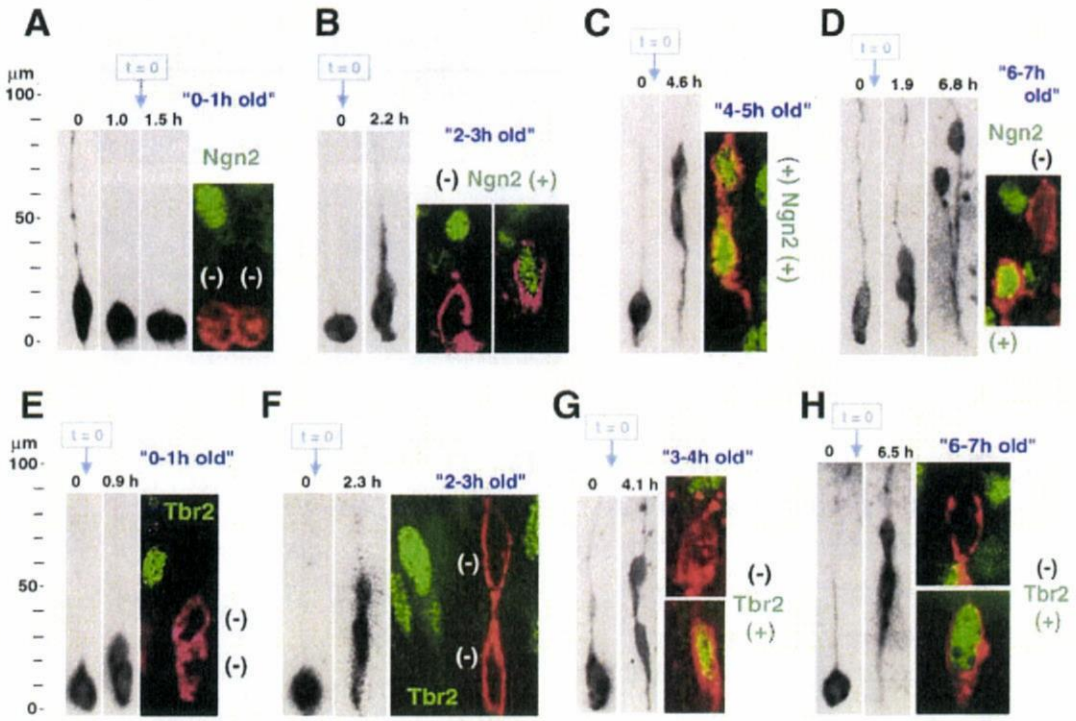
A
B
C
D
μm
100
50
0
t = 0
"0-1h old"
0 1.0 1.5 h
Ngn2
(-) (-)
"2-3h old"
0 2.2 h
(-) Ngn2 (+)
"4-5h old"
0 4.6 h
(+) Ngn2 (+)
"6-7h old"
0 1.9 6.8 h
Ngn2
(-)
(+)
E
F
G
H
"0-1h old"
0 0.9 h
Tbr2
(-)
(-)
"2-3h old"
0 2.3 h
(-)
(-)
Tbr2
"3-4h old"
0 4.1 h
(-)
Tbr2
(+)
"6-7h old"
0 6.5 h
(-)
Tbr2
(+)

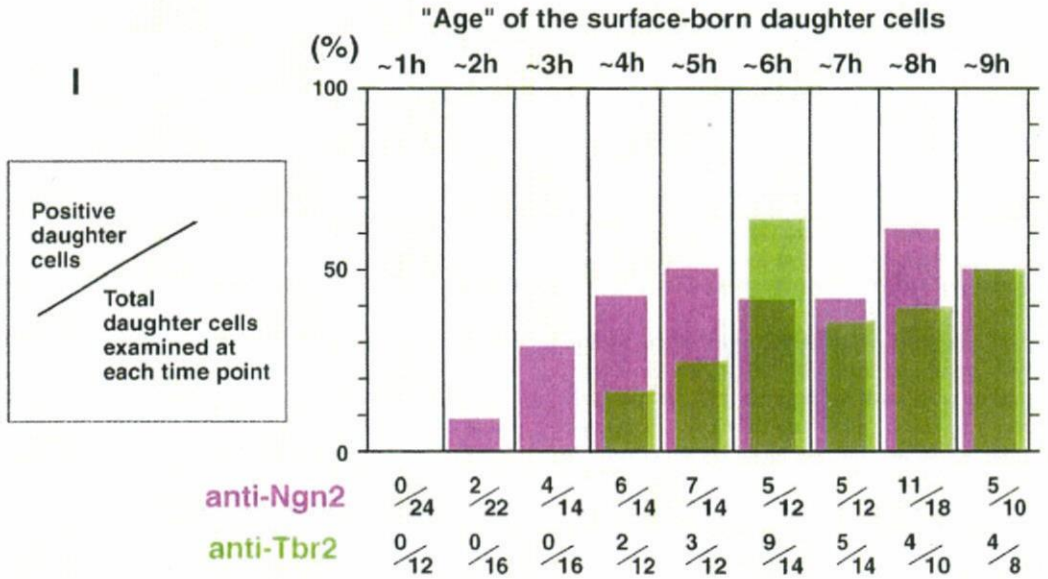
I
"Age" of the surface-born daughter cells
(%)
~1h ~2h ~3h ~4h ~5h ~6h ~7h ~8h ~9h
100
50
0
Positive daughter cells
Total daughter cells examined at each time point
anti-Ngn2
0/24 2/22 4/14 6/14 7/14 5/12 5/12 11/18 5/10
anti-Tbr2
0/12 0/16 0/16 2/12 3/12 9/14 5/14 4/10 4/8

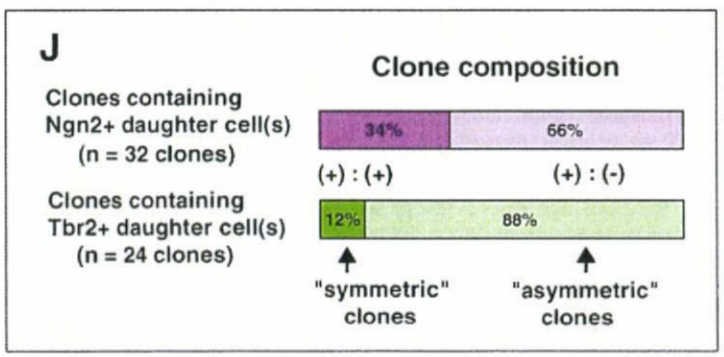
J
Clone composition
Clones containing Ngn2+ daughter cell(s) (n = 32 clones)
34%
66%
(+) : (+)
(+) : (-)
Clones containing Tbr2+ daughter cell(s) (n = 24 clones)
12%
88%
"symmetric" clones
"asymmetric" clones

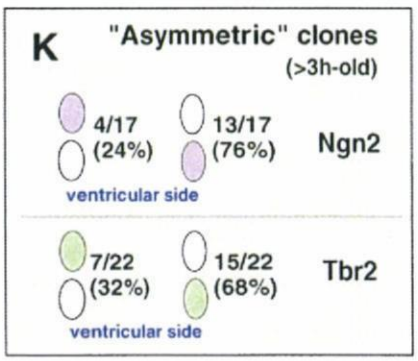
K
"Asymmetric" clones
(>3h-old)
4/17 (24%)
13/17 (76%)
Ngn2
ventricular side
7/22 (32%)
15/22 (68%)
Tbr2
ventricular side

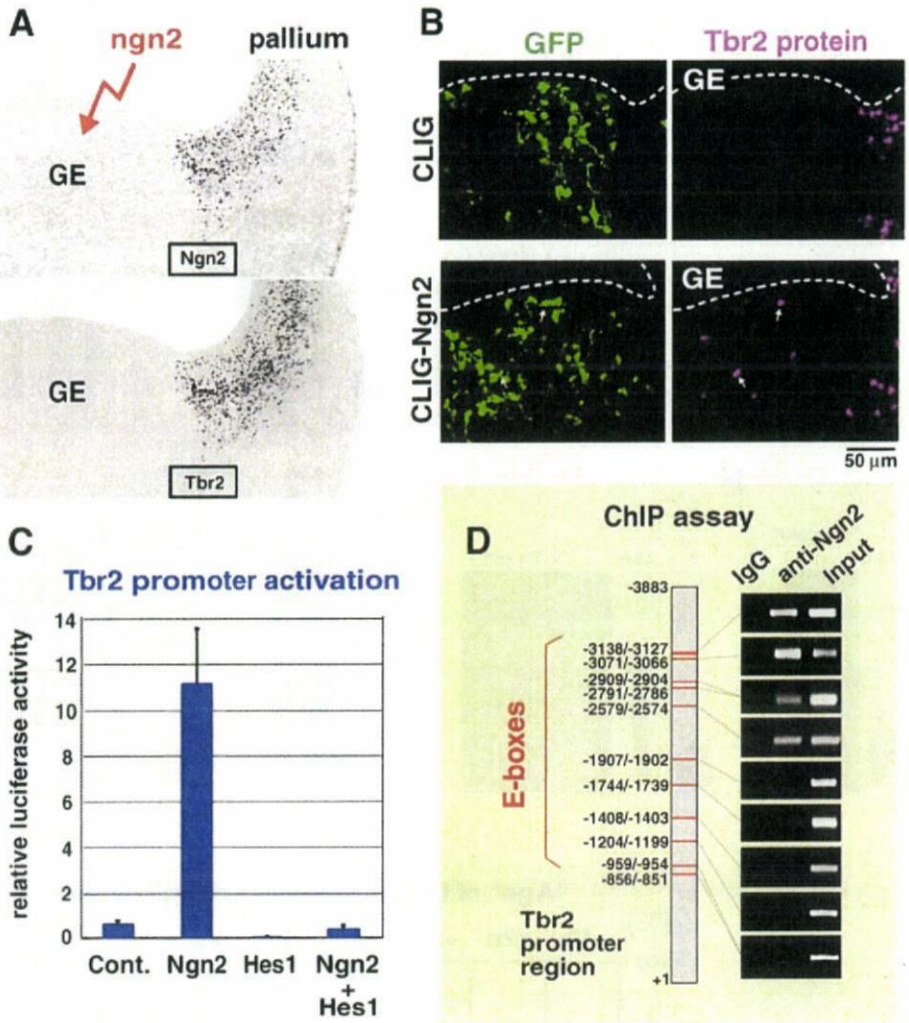

Fig. 3. Ngn2 directly upregulates Tbr2 expression. (A) Ectopic expression of Ngn2 in the E13 ganglionic eminence (GE) by electroporation (EP) to test whether it induces Tbr2 expression. Note that both proteins are normally absent from the GE. (B) 24 h after EP with CLIG-Ngn2, 8.9% (n=1340) of GFP$^+$ cells in the GE were also Tbr2$^+$, whereas all GFP$^+$ GE cells were Tbr2-negative when electroporated with a control vector (CLIG, n=454). (C) EP-based luciferase assay using VZ cells of the GE. Ngn2, but not Hes1 or Ngn2+Hes1, significantly induced luciferase activation. Similar results were obtained using VZ cells of the pallium (Fig. S4B). (D) Chromatin immunoprecipitation (ChIP) assay showing *in vivo* binding of the Ngn2 protein to the Tbr2 promoter. Immunoprecipitate prepared using anti-Ngn2 antibody was subjected to PCR using primers flanking the E-boxes (red lines) of the Tbr2 promoter.

The initial morphology of daughter cells that subsequently moved to the SVZ and divided to generate neurons was frequently pin-like in regions of the E14 cerebral wall with a thickness of approximately 200 μm (Fig. 1A; Miyata et al., 2004). Our observation that Ngn2 and Tbr2 are expressed in the apical and not the basal daughter cells in 200 μm thick cerebral wall regions (Fig. 2K) is consistent with the model that the Ngn2-Tbr2 cascade plays a role in allocating one of the daughter cells born in the VZ of this cerebral wall region to the SVZ and to a neuronal lineage.

We also observed that neuron pairs were produced by cells that initially had radial glial morphology, but subsequently underwent a bipolar-to-unipolar transition upon losing their ventricular connection and moved to the SVZ (Figs. S4A, B) (Miyata et al., 2001; Miyata and Ogawa, 2007). Although these cells tended to be observed in a thinner (140 μm) and less developmentally advanced region of the cerebral wall (Miyata et al., 2004), they were also present in slightly thicker areas (Fig. S4), consistent with detection of Ngn2 expression in some of the basal daughters (Fig. 2K).

Asymmetric Ngn2 initiation precedes p27 expression

To identify candidate factors that might induce asymmetric Ngn2 expression within clones, we first focused on the cell cycle inhibitor p27, which has been shown to stabilize Ngn2. The loss of p27 leads to a reduction in Ngn2-positive VZ/SVZ cells (Nguyen et al., 2006), and treatment of the telencephalon with cell cycle inhibitors promotes

Fig. 2. Expression of Ngn2 or Tbr2 protein in age-tracked daughter cells. (A–H) Expression of Ngn2 (A–D, green) or Tbr2 (E–H, green) in two-cell clones generated at the ventricular surface of cultured cerebral wall slices. Time-lapse imaging from mitosis of a DiI-labeled founder progenitor cell until various time points up to about 9 h was performed, followed by vibratome sectioning of slices and immunostaining of daughter cells. To ensure viability of M-phase cells and the production of healthy daughter cells, cells were usually imaged only once or twice during M-phase, and the time from birth of each daughter cell (i.e. division of its parent cell) was estimated by defining anaphase (B) and cytokinesis (H) as time zero (t=0). Metaphase, which could be identified by the existence of a DiI-negative "metaphase plate" within a round soma (E, F), was observed 15–20 min before time zero, and prophase/prometaphase cells, whose somata were more elliptical (A, C, D, G), were observed 30–50 min before time zero. The total M-phase duration in slice cultures was usually about 1–1.2 h, with anaphase lasting only about 10 min (Miyata et al., 2001). Given these technical and biological considerations, daughter cell ages were estimated with a resolution of 1 h and grouped into nine categories (140 cells for Ngn2 immunostaining and 114 cells for Tbr2 immunostaining). (I) Histogram showing age-dependent expression of Ngn2 or Tbr2 proteins. Each column represents the proportion of daughter cells that were positive for Ngn2 (magenta) or Tbr2 (green) at each age. (J) Summary of the composition of clones that contained immunopositive cell(s). (K) Spatial dissection of clones in which Ngn2 or Tbr2 was asymmetrically expressed. Both Ngn2 and Tbr2 were seen more frequently in the apical daughter cell than in the basal daughter cell.

neuronal differentiation (Calegari and Huttner, 2003). To determine whether p27 expression precedes Ngn2 expression, we carried out anti-p27 immunofluorescence using a monoclonal antibody whose specificity was confirmed using p27−/− mice (Nagahama et al., 2001). Double immunostaining of frozen sections revealed that some Ngn2$^+$ cells were also p27$^+$ (Figs. S4A, E), but double positive cells were all within the SVZ or upper VZ, not in the periventricular area (lower VZ) where Ngn2 expression begins, confirming a previous report (Kawaguchi et al., 2004; Nguyen et al., 2006). Ngn2$^+$ cells in the periventricular area were instead positive for cyclinD1 (Figs. S4A, F) and Ki67 (Figs. S4A, C, D), markers of cycling cells. These data indicate that p27 does not initiate Ngn2 expression in VZ cells.

Short-term pharmacological inhibition of Notch signaling results in premature Ngn2 expression in nascent daughter cells

To determine what controls the onset of Ngn2 protein expression 2 h after daughter cell birth, we next focused on Notch signaling. Previous immunohistochemical analysis using an anti-Notch intracellular domain (anti-NICD) (Tokunaga et al., 2004) or anti-Hes1 (Shimojo et al., 2008) antibody demonstrated that nuclei with strong Notch activation were located in the upper half of the VZ, with a distribution pattern complementary to that of Ngn2 protein. However, it is possible that Notch signaling is weakly activated at an earlier stage in the lower VZ, where Ngn2 expression is not observed or only gradually initiated.

To determine whether loss of Notch signaling affects the timing of Ngn2 expression in nascent daughter cells, slices containing daughter cell clones were treated with compound E (CpdE), a γ-secretase inhibitor (Zhao et al., 2005). We first identified DiI-labeled M-phase cells and added CpdE to the culture, fixed the CpdE-treated slice 2 or 3 h later, and examined whether DiI-labeled daughter cells were Ngn2 immunoreactive (Figs. 4A, B). If the frequency of Ngn2 expression in 2 or 3 h-old daughter cells exposed to CpdE from their birth were similar to that of control daughter cells, Notch signaling would not be likely to play an important role during this time on expression of Ngn2 in nascent daughter cells. If, however, the frequency of Ngn2 expression significantly

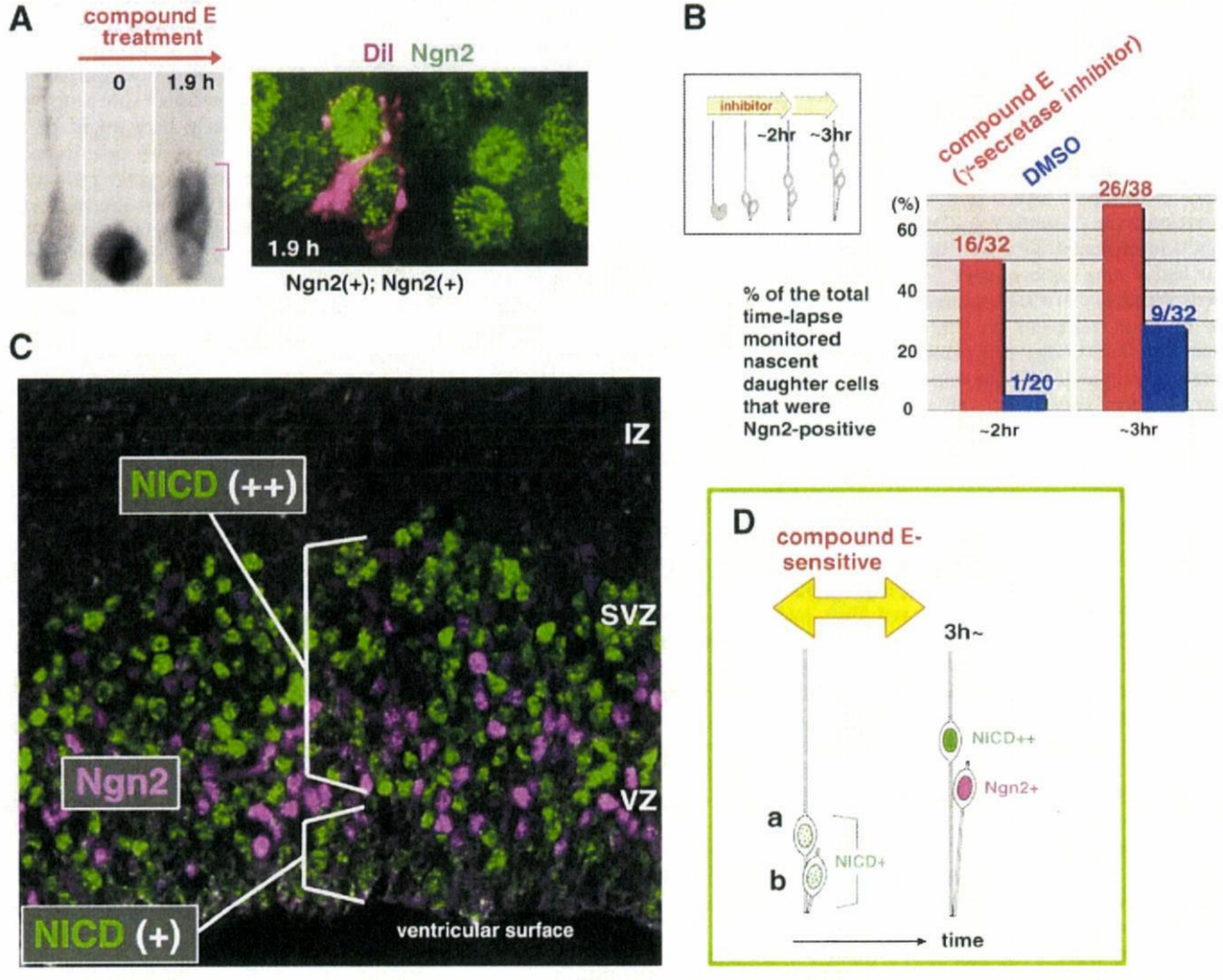

Fig. 4. Notch signaling prevents the youngest daughter cells from prematurely expressing Ngn2 in the periventricular area. (A, B) Short-term pharmacological treatment of cerebral wall slices with a γ-secretase inhibitor (compound E) resulted in more frequent and earlier Ngn2 expression in the time-lapse monitored nascent daughter cells. Compound E (5 μM) or DMSO (0.05%) was added to slice cultures shortly after division of a DiI-labeled progenitor cell was observed at the ventricular surface (time 0 in the left panel of A). Slices were fixed after about 2 or 3 h and further processed for Ngn2 immunostaining (A, right). Age determination was more precise than in the histogram in Fig. 2 as a result of more frequent time-lapse observation during the M phase. At both 2 and 3 h, the percentage of the total monitored daughter cells that was positive for Ngn2 was significantly greater in the compound E-treated group than in the DMSO-treated group (B, $p<0.001$, chi-square test). (C) Immunoreactivity for the Notch1 intracellular domain (N1ICD) (green) was intense in the basal half of the VZ of E14 cerebral walls, but was also weakly detected in the apical part of the VZ. N1ICD immunoreactivity did not overlap with Ngn2 immunoreactivity (magenta). (D) Schematic diagram showing the relationship between cellular morphology, the expression of N1ICD, the expression of Ngn2, and the results of the compound E experiments. Somata of the nascent daughter cells (RG-like daughter cell a and short pin-like daughter cell b) reside in the periventricular area, where a moderate level of N1ICD immunoreactivity is detected (C). Note that although this panel summarizes the effects of short-term pharmacological treatment (yellow double-headed arrow), VZ cells older than 3 h are also sensitive to compound E treatment (see Fig. S5A).

increased, this would demonstrate that Notch signaling functions during this early time window. Strikingly, the CpdE-treated nascent daughter cells were positive for Ngn2 much more frequently than the control DMSO-treated cells (50% in CpdE vs. 5% in DMSO at 2 h and 68% in CpdE vs. 28% in DMSO at 3 h, both $p<0.001$ by chi-square test).

In 2 h-old CpdE-treated daughter cells, the average distance of $Ngn2^+$ nuclei ($n=16$) from the ventricular surface was 18 ± 11 μm, with seven nuclei observed within 10 μm from the surface. Longer CpdE treatment further increased the number of $Ngn2^+$ cells (3–12 h), and later the number of $Tbr2^+$ cells (12–24 h), throughout the VZ (Fig. S5A). We next assessed the intraclonal asymmetry of Ngn2 in the CpdE-treated clones (11 clones at 2 h-old and 18 clones at 3 h-old). Clones in which both daughter cells were $Ngn2^+$ were more frequently found (45% [5/11] at 2 h and 53% [9/17] at 3 h) than in DMSO-treated 3 h-old clones (29%, $n=7$ clones). In the remaining CpdE-treated clones that had only one $Ngn2^+$ daughter cell (6 clones at 2 h-old and 9 clones at 3 h-old), the frequency of Ngn2 expression was almost equal between the basal and apical nuclei (50% vs. 50% [$n=6$ nuclei] at 2 h and 44% vs. 56% [$n=9$ nuclei] at 3 h), whereas it was higher in the apical nuclei (80%) of control DMSO-treated asymmetric clones ($n=5$ clones), similar to what was observed in asymmetric clones that did not receive pharmacological treatment (Fig. 2J).

To confirm Notch activation in nascent daughter cells, we visualized the distribution of the intracellular domain of Notch1 (N1ICD) using an immunohistochemical method with improved sensitivity (Del Monte et al., 2007). Consistent with previous reports (Tokunaga et al., 2004), N1ICD immunoreactivity was intense in the upper portion of the VZ, while $Ngn2^+$ nuclei were N1ICD-negative (Fig. 4C). N1ICD immunoreactivity was also detected at low levels in the periventricular area, where very few, if any, $Ngn2^+$ cells were observed. Notably, N1ICD immunoreactivity was considerably reduced by CpdE treatment for 2 h and it was completely lost by CpdE treatment for 3 h (Fig. S5B). Taken together, these results suggest that Notch activation during the initial phase of life in surface-born daughter cells may prevent the initiation of the Ngn2-Tbr2 cascade that would otherwise commit them to the neuronal lineage.

Discussion

By immunostaining neocortical daughter cell pairs that were individually labeled and time-lapse monitored from their birth in 3D cultured slices, we were able to obtain an expression timeline for the neurogenic transcription factors Ngn2 and Tbr2. We have demonstrated that within 2 h after birth, both factors are absent from daughter cells, but Ngn2 expression is soon thereafter initiated in an intraclonally asymmetric pattern, followed by a similar pattern of Tbr2 expression 2 h later. We showed that Ngn2 directly activates the Tbr2 promoter, and that Notch signaling is activated in nascent daughter cells to prevent the initiation of the Ngn2-Tbr2 cascade. This is the first examination of the inter- and intracellular molecular events during the earliest stages of daughter cell development.

Our time-lapse observation of the behavior of daughter cells generated at the ventricular surface (Fig. 1A) raises the question of why cells that eventually move to the SVZ to undergo mitosis or neuronal differentiation are initially connected to the ventricular surface. The present study suggests that the initial surface-connected morphology is important for nascent daughter cells to receive Notch ligands presented in the periventricular area. Nascent daughter cells connected to the ventricular surface either resemble radial glia (RG) reflecting their inheritance of a pial process or have a short pin-like morphology due to lack of an inherited pial process (Fig. 1A; schematically illustrated in Fig. 4D). Not only RG-like cells but also short pin-like cells were sensitive to γ-secretase inhibition, resulting in premature and more frequent expression of Ngn2 (Figs. 4A, B). Moreover, N1ICD was detected in the periventricular area (Fig. 4C). Consistent with this data, recent immunohistochemical examinations on the expression of Delta-like-1 in mouse cerebral walls have suggested that it is expressed periventricularly, not in the basal (pial) domain containing fully differentiated neurons (Yoshimatsu et al., 2006; Kawaguchi et al., 2008; Nakatani et al., unpublished). Furthermore, studies focusing on the subtype of progenitor cells have recently demonstrated that the intermediate/basal progenitors immediately after commitment to the neuronal lineage express Delta within the VZ (Kawaguchi et al., 2008; Yoon et al., 2008). Ngn2 expression starts in surface-born cells that are still connected to the ventricular surface (Figs. 2, 4, S1) and Ngn2 directly induces Delta expression (Castro et al., 2006), suggesting that the initial attachment of VZ cells to the ventricle is important for the presentation of Delta in the periventricular area. Taken together, the initial possession of an apical process by almost all surface-born daughter cells may ensure the Notch-based maintenance of a self-renewing and proliferating population to avoid premature depletion of progenitors during early and mid stages of neocortical neurogenesis.

How the intraclonally asymmetric Ngn2 expression occurs is still unclear. Our experiments have shown that soon after birth, daughter cells treated with a γ-secretase inhibitor prematurely express Ngn2. This responsiveness of daughter cells can be interpreted in two different ways. It is possible that daughter cells 2 h-old and younger are completely neutral and are not biased towards expressing Ngn2 or towards the neuronal lineage. Alternatively, they might be biased towards the neuronal lineage but not irrevocably determined. One intriguing possibility is that pair-generated daughter cells differentially activate Notch signaling depending on their morphology. It is possible that a greater amount of Delta is presented to the RG-like daughter cells than to the much shorter pin-like cells, leading to stronger activation of Notch signaling and asymmetric fate choices. This model of cell fate regulation through morphology-dependent, differential Delta–Notch interaction is consistent with the observations that apical daughter cells are more frequently $Ngn2^+$ than basal cells (Fig. 2J) and that pin-like cells move to the SVZ for abventricular mitosis more frequently than RG-like cells in cerebral walls about 200 μm thick (Miyata et al., 2004). It is also consistent with a recent suggestion by Konno et al. (2008) that the basal compartment of a daughter cell may be important for its progenitor fate choice. However, other mechanisms might also exist, because the opposite pattern of intraclonal asymmetry (i.e. asymmetric Ngn2 expression by the basal daughter cell (Fig. S3) and migration of RG-like cells to the SVZ (Miyata et al., 2001, 2004; Miyata and Ogawa, 2007)) have also been observed. We also do not exclude the possibility that cell fate biasing events may initiate before the birth of daughter cells, i.e. within M-phase cells.

Unfortunately, it has not been possible so far for us to directly assess whether the degree of Notch activation is asymmetric in a single clone less than 2 h old due to technical difficulties in simultaneously detecting DiI and N1ICD. Live monitoring of Notch activity in 3D tissues with single cell resolution using GFP-derivatives under the regulation of Hes promoters (Koyama et al., 2005; Ohtsuka et al., 2006) or a CBF1-responsive element (Mizutani et al., 2007) would be very fruitful. Recently, live luciferase assays using monolayer cultured neocortical cells showed that cells that have not yet committed to the neuronal lineage activate the Hes1 and Ngn2 promoters in inverse oscillatory patterns, and that Ngn2-luciferase signal ceased to oscillate and became persistent upon neuronal lineage commitment (Shimojo et al., 2008). It would be interesting to examine how such oscillatory patterns of expression relate to the timeline of Ngn2 and Tbr2 that we obtained from immunostaining *in situ*.

Experimental methods

Slice culture

DiI-labeled slices prepared from the dorsal region of E14 cerebral walls were cultured in collagen gel, as previously described (Miyata

et al., 2001, 2004). To follow "pin-like" cells that were connected only to the ventricular surface, a suspension of extremely fine DiI crystals (<5 μm in diameter) in DMEM/F12 (Saito et al., 2003) was injected into lateral ventricles, followed by slice preparation. In CpdE-treatment experiments (Fig. 4), time-lapse images were obtained at shorter time intervals than used for the expression timeline (Fig. 2), for more accurate staging of daughter cells. Detailed information for the imaging is available in the Supplemental methods.

Immunohistochemistry

Frozen sections of cerebral walls and vibratome or frozen sections prepared from cultured slices were immunostained with the following antibodies: Ki67 (mouse IgG, Novocastra), cyclinD1 (rabbit, Lab Vision), p27 (mouse IgG, Transduction laboratories), BrdU (mouse IgG, Sigma), GFP (rabbit, MBL), Ngn2 (mouse IgG, gift from Dr. David Anderson [Lo et al., 2002]; rabbit, gift from Dr. Masato Nakafuku [Mizuguchi et al., 2001]), Tbr2 (rabbit, gift from Dr. Robert Hevner), Pax6 (rabbit, Covance), and N1ICD (rabbit, Cell Signaling). For anti-N1ICD immunostaining, frozen sections were pre-treated with citrate buffer (at 105 °C for 5 min) and signal was enhanced using a tyramide signal amplification kit (TSA-Plus Fluorescein System, Perkin Elmer) as previously described (Del Monte et al., 2007). Immunostaining of DiI-labeled slices was performed as previously described (Miyata et al., 2001). Briefly, slices were fixed in 4% paraformaldehyde for 15 min at room temperature, vibratome sectioned (50 μm), and treated with antibodies (4 °C, 8–10 h), and subjected to confocal microscopy. For the histograms in Figs. 1E and 4A, values obtained from three independent E14 embryos were averaged (>500 VZ/SVZ cells were counted in each section of the dorsal region of the cerebral wall).

Electroporation

E13 cerebral hemispheres were electroporated with pCS2-myc-Ngn2 (gift from Dr. Jacqueline E. Lee), pCLIG-Ngn2, pCLIG-Math3 (gift from Dr. Ryoichiro Kageyama), using a CUY21E electroporator (Neppa gene, Japan), and slices of hemispheres containing the lateral or caudal ganglionic eminence were cultured as described above.

Luciferase assay

E13 cerebral walls (pallial region or ganglionic eminence region) were electroporated with pGV-DBH-Tbr2 (containing a firefly luciferase gene under the Tbr2 promoter, gift from Dr. Tetsuya Taga), pCS2-Ngn2, and pCMV-Renilla, dissociated into single cells, then cultured for 24 h in 24-well plates coated with poly-L-ornithine (Sigma) and fibronectin (Invitrogen). Cell lysates were made using the Dual-Luciferase Assay system (Promega) and transferred to 96-well plates. Luciferase activity of each lysate was measured in triplicate by a luminometer (Luminoskan Ascent Type 392, Labsystems). Firefly luciferase activity was normalized relative to the activity of *Renilla* luciferase.

Chromatin immunoprecipitation (ChIP) assay

Immunoprecipitation was carried out using an anti-Ngn2 antibody (gift from Dr. David Anderson, Lo et al., 2002). Detailed information is available in the Supplemental methods.

Pharmacology

For experiments to block Notch activity, we used compound E (CpdE; Calbiochem, 5 μM), which is known to inhibit γ-secretase at a much lower dose than DAPT (Zhao et al., 2005).

Acknowledgments

We thank Rovert Hevner, David J. Anderson, Tetsuya Taga, and Ryoichiro Kageyama for antibodies and plasmids, Young-Yun Kong and Ayano Kawaguchi for critical reading of the manuscript, and Jacqueline E. Lee for inspiration and encouragement. This work was supported by grants from the Japanese Ministry of Education, Science, Sports and Culture (No. 20021016), Takeda Science Foundation, Toyo-Aki Foundation, and Kanahara Foundation.

Appendix A. Supplementary data

Supplementary data associated with this article can be found, in the online version, at doi:10.1016/j.mcn.2008.10.007.

References

Arnold, S.J., Huang, G.-J., Cheung, A.F.P., Era, T., Nishikawa, S.-I., Bikoff, E.K., Molnar, Z., Robertson, E.J., Groszer, M., 2008. The T-box transcription factor Eomes/Tbr2 regulates neurogenesis in the cortical subventricular zone. Genes Dev. 22, 2479–2484.

Baala, L., Briault, S., Etchevers, H.C., Laumonnier, F., Natiq, A., Amiel, J., Boddaert, N., Picard, C., Sbiti, A., Asermouth, A., Attie-Bitach, T., Encha-razavi, F., Munnich, A., Sefiani, A., Lyonnet, S., 2007. Homozygous silencing of T-box transcription factor EOMES leads to microcepjaly with polymicrogyria and corpus callosum agenesis. Nat. Genet. 39, 454–456.

Cai, L., Hayes, N.L., Takahashi, T., Caviness Jr., V.S., Nowakowski, R.S., 2002. Size distribution of retrovirally marked lineages matches prediction from population measurements of cell cycle behavior. J. Neurosci. Res. 69, 731–744.

Calegari, F., Huttner, W.B., 2003. An inhibitor of cyclin-dependent kinases that lengthens, but does not arrest, neuroepithelial cell cycle induces premature neurogenesis. J. Cell. Sci. 116, 4947–4955.

Castro, D.S., Skowronska-Krawczyk, D., Armant, O., Donaldson, I.J., Parras, C., Hunt, C., Critchley, J.A., Nguyen, L., Gossler, A., Gottgens, B., Matter, J.-M., Guillemot, F., 2006. Proneural bHLH and Brn proteins coregulate a neurogenic program through cooperative binding to a conserved DNA motif. Dev. Cell 11, 831–844.

Chenn, A., McConnell, S.K., 1995. Cleavage orientation and the asymmetric inheritance of Notch1 immunoreactivity in mammalian neurogenesis. Cell 82, 631–641.

Del Bene, F., Wehman, A.M., Link, B.A., Baier, H., 2008. Regulation of neurogenesis by interkinetic nuclear migration through an apical-basal Notch gradient. Cell 134, 1055–1065.

Del Monte, G., Grego-Bessa, J., Gonzaralez-Rajal, A., Bolos, V., De La Pompa, J.L., 2007. Monitoring Notch1 activity in development: evidence for a feedback regulatory loop. Dev. Dyn. 236, 2594–2614.

Doe, C.Q., 2008. Neural stem cells: balancing self-renewal with differentiation. Development 135, 1575–1587.

Englund, C., Fink, A., Lau, C., Pham, D., Daza, R.A., Bulfone, A., Kowalczyk, T., Hevner, R.F., 2005. Pax6, Tbr2, and Tbr1 are expressed sequentially by radial glia, intermediate progenitor cells, and postmitotic neurons in developing neocortex. J. Neurosci. 25, 247–251.

Gaiano, N., Fishell, G., 2002. The role of notch in promoting glial and neural stem cell fates. Annu. Rev. Neurosci. 25, 471–490.

Ge, W., He, F., Kim, K.J., Blanchi, B., Coskun, V., Nguyen, L., Wu, X., Zhao, J., Heng, J.I.-T., Martinowich, K., Tao, J., Wu, H., Castro, D., Sobeih, M.M., Corfas, G., Gleeson, J.G., Greenberg, M.E., Guillemot, F., Sun, Y.E., 2006. Coupling of cell migration with neurogenesis by proneural bHLH factors. Proc. Natl. Acad. Sci. U. S. A. 103, 1319–1324.

Guillemot, F., 2007. Spatial and temporal specification of neural fates by transcription factor codes. Development 134, 3771–3780.

Hand, R., Bortone, D., Mattar, P., Nguyen, L., Heng, J.I.-T., Guerrier, S., Boutt, E., Peters, E., Barnes, A.P., Parras, C., Schuurmans, C., Guillemot, F., Polleux, F., 2005. Phosphorylation of Neurogenin2 specifies the migration properties and the dendritic morphology of pyramidal neurons in the neocortex. Neuron 48, 45–62.

Harris, W.A., Holt, C.E., 1990. Early events in the embryogenesis of the vertebrate visual system: cellular determination and pathfinding. Annu. Rev. Neurosci. 13, 155–169.

Haubensak, W., Attardo, A., Denk, W., Huttner, W.B., 2004. Neurons arise in the basal neuroepithelium of the early mammalian telencephalon: a major site of neurogenesis. Proc. Acad. Natl. Sci. U. S. A. 101, 3196–3201.

Hayder, T.F., Ang Jr., E., Rakic, P., 2003. Mitotic spindle rotation and mode of cell division in the developing telencephalon. Proc. Natl. Acad. Sci. U. S. A. 100, 2890–2895.

Kageyama, R., Otsuka, T., Hatakeyama, J., Ohsawa, R., 2005. Role of bHLH genes in neural stem cell differentiation. Exp. Cell Res. 306, 343–348.

Kawaguchi, A., Ogawa, M., Saito, K., Matsuzaki, F., Okano, H., Miyata, T., 2004. Differential expression of Pax6 and Ngn2 between pair-generated cortical neurons. J. Neurosci. Res. 78, 784–795.

Kawaguchi, A., Ikawa, T., Kasukawa, T., Ueda, H.R., Kurimoto, K., Saitou, M., Matsuzaki, F., 2008. Single-cell gene profiling defines differential progenitor subclasses in mammalian neurogenesis. Development 135, 3113–3124.

Knoblich, J.A., 2008. Mechanism of asymmetric stem cell division. Cell 132, 583–597.

Kohyama, J., Tokunaga, A., Fujita, Y., Miyoshi, H., Nagai, T., Miyawaki, A., Nakao, K., Matsuzaki, Y., Okano, H., 2005. Visualization of spatiotemporal activation of Notch

signaling: live monitoring and significance in neural development. Dev. Biol. 286, 311–325.
Konno, D., Shioi, G., Shitamukai, A., Mori, A., Kiyonari, H., Miyata, T., Matsuzaki, F., 2008. Neuroepithelial progenitors undergo LGN-dependent planar divisions to maintain self-renewability during mammalian neurogenesis. Nat. Cell Biol. 10, 93–101.
Kosodo, Y., Roper, K., Haubensak, W., Marzesco, A.-M., Corbeil, D., Huttner, W., 2004. Asymmetric distribution of the apical plasma membrane during neurogenic divisions of mammalian neuroepithelial cells. EMBO J. 23, 2314–2324.
Landrieu, P., Goffinet, A., 1979. Mitotic spindle fiber orientation in relation to cell migration in the neo-cortex of normal and reeler mouse. Neurosci. Lett. 13, 69–72.
Lo, L., Dormand, E., Greenwood, A., Anderson, D.J., 2002. Comparison of the generic neuronal differentiation and neuron subtype specification functions of mammalian achaete-scute and atonal homologues in cultured neural progenitor cells. Development 129, 1553–1567.
McConnell, S.K., 1991. The generation of neuronal diversity in the central nervous system. Annu. Rev. Neurosci. 14, 269–300.
Miyata, T., Ogawa, M., 2007. Twisting of neocortical progenitor cells underlies a spring-like mechanism for daughter-cell migration. Curr. Biol. 17, 146–151.
Miyata, T., Kawaguchi, A., Okano, H., Ogawa, M., 2001. Asymmetric inheritance of radial glial fibers by cortical neurons. Neuron 31, 727–741.
Miyata, T., Kawaguchi, A., Saito, K., Kawano, M., Muto, T., Ogawa, M., 2004. Asymmetric production of surface-dividing and non-surface-dividing cortical progenitor cells. Development 131, 3133–3145.
Mizuguchi, R.M., Sugimori, H., Takebayashi, H., Kosako, M., Nagao, S., Yoshida, Y., Nabeshima, Y., Shimamura, K., Nakafuku, M., 2001. Combinational roles of olig2 and neurogenin2 in the coordinated induction of panneuronal and subtype-specific properties of motoneurons. Neuron 31, 757–771.
Mizutani, K., Yoon, K., Dang, L., Tokunaga, A., Gaiano, N., 2007. Differential Notch signaling distinguishes neural stem cells from intermediate progenitors. Nature 449, 351–355.
Murciano, A., Zamora, J., Lopes-Sanchez, J., Frade, J.M., 2002. Interkinetic nuclear movement may provide spatial clues to the regulation of neurogenesis. Mol. Cell. Neurosci. 21, 285–300.
Nagahama, H., Hatakeyama, S., Nakayama, K., Nagata, M., Tomita, K., Nakayama, K., 2001. Spatial and temporal expression patterns of the cyclin-dependent kinase (CDK) inhibitors p27Kip1 and p57Kip2 during mouse development. Anat. Embryol. 203, 77–87.
Nguyen, L., Besson, A., Heng, J.I.-T., Shuurmans, C., Teboul, L., Parras, C., Philpott, A., Robertis, J.M., Guillemot, F., 2006. $p27^{kip1}$ independently promotes neuronal differentiation and migration in the cerebral cortex. Genes Dev. 20, 1511–1524.
Nieto, M., Shuurmans, C., Britz, O., Guillemot, F., 2001. Neural bHLH genes control the neuronal versus glial fate decision in cortical progenitors. Neuron 29, 401–413.
Nishizawa, Y., Imafuku, H., Saito, K., Kanda, R., Kimura, M., Minobe, S., Miyazaki, F., Kawakatsu, S., Masaoka, M., Ogawa, M., Miyata, T., 2007. Survey of the morphogenetic dynamics of the ventricular surface of the developing mouse neocortex. Dev. Dyn. 236, 3061–3070.
Noctor, S.C., Flint, A.C., Weissman, T.A., Dammerman, R.S., Kriegstein, A.R., 2001. Neurons derived from radial glial cells establish radial units in neocortex. Nature 409, 714–720.
Noctor, S.C., Martinez-Cerdeno, V., Ivic, L., Kriegstein, A.R., 2004. Cortical neurons arise in symmetric and asymmetric division zones and migrate through specific phases. Nat. Neurosci. 7, 136–144.
Noctor, S.C., Martinez-Cerdeno, V., Kriegstein, A.R., 2008. Distinct behaviors of neural stem and progenitor cells underlie cortical neurogenesis. J. Comp. Neurol. 508, 28–44.
Ochiai, W., Minobe, S., Ogawa, M., Miyata, T., 2007. Transformation of pin-like ventricular zone cells into cortical neurons. Neurosci. Res. 57, 326–329.
Ohtsuka, T., Imayoshi, I., Shimojo, H., Nishi, E., Kageyama, R., McConnell, S.K., 2006. Mol. Cell. Neurosci. 31, 109–122.
Saito, K., Kawaguchi, A., Kashiwagi, S., Yasugi, S., Ogawa, M., Miyata, T., 2003. Dev. Growth Differ. 45, 219–229.
Sanada, K., Tsai, L.-H., 2005. G protein βγ subunits and AGS3 control spindle orientation and asymmetric cell fate of cerebral cortical progenitors. Cell 122, 119–131.
Sessa, A., Mao, C., Hadjantonakis, A.-K., Klein, W.H., Broccoli, V., 2008. Tbr2 directs conversion of radial glia into basal precursors and guides neuronal amplification by indirect neurogenesis in the developing neocortex. Neuron 60, 56–69.
Shimojo, H., Ohtsuka, T., Kageyama, R., 2008. Oscillations in Notch signaling regulate maintenance of neural progenitors. Neuron 58, 52–64.
Shuurmans, C., Armant, O., Nieto, M., Stenman, J.M., Britz, O., Klenin, N., Brown, C., Langevin, L.-M., Seibt, J., Tang, H., Cunningham, J.M., Dyck, R., Walsh, C., Campbell, K., Polleux, F., Guillemot, F., 2004. Sequential phases of cortical specification involve *Neurogenin*-dependent and -independent pathways. EMBO J. 23, 2892–2902.
Smart, I.H.M., 1973. Proliferative characteristics of the ependymal layer during the early development of the mouse neocortex: a pilot study based on recording the number, location and plane of cleavage of mitotic figures. J. Anat. 116, 67–91.
Takahashi, T., Nowakowski, R.S., Caviness Jr., V.S., 1996. The leaving or Q fraction of the murine cerebral proliferative epithelium: a general model of neocortical neuronogenesis. J. Neurosci. 16, 6183–6196.
Temple, S., 1990. Characteristics of cells that give rise to the central nervous system. J. Cell. Sci. 97, 213–218.
Tokunaga, A., Kohyama, J., Yoshida, T., Nakao, K., Sawamoto, K., Okano, H., 2004. Mapping spatio-temporal activation of Notch signaling during neurogenesis and gliogenesis in the developing mouse brain. J. Neurochem. 90, 142–154.
Ueno, M., Kimura, N., Nakashima, K., Saito-Ohara, F., Inazawa, J., Taga, T., 2000. Genomic organization, sequence and chromosomal localization of the mouse Tbr2 gene and a comparative study with Tbr1. Gene 254, 29–35.
Yoon, K.-J., Koo, B.-K., Im, S.-K., Jeong, H.-W., Ghim, J., Kwon, M., Moon, J.-S., Miyata, T., Kong, Y.-Y., 2008. Mind bomb 1-expressing intermediate progenitors generate Notch signaling to maintain radial glial cells. Neuron 58, 519–531.
Yoshimatsu, T., Kawaguchi, D., Oishi, K., Takeda, K., Akira, S., Masuyama, N., Gotoh, Y., 2006. Non-cell-autonomous action of STAT3 in maintenance of neural precursor cells in the mouse neocortex. Development 133, 2553–2563.
Zhao, G., Cui, M.-Z., Mao, G., Dong, Y., Tan, J., Sun, L., Xu, X., 2005. γ-cleavage is dependent on ζ-cleavage during the proteolytic processing of amyloid precursor protein within its transmembrane domain. J. Biol. Chem. 280, 37689–37697.
Zhong, W., Feder, J.N., Jiang, M.M., Jan, L.Y., Jan, Y.N., 1996. Asymmetric localization of a mammalian numb homolog during mouse cortical neurogenesis. Neuron 17, 43–53.

Epigenetic regulation of neural cell differentiation plasticity in the adult mammalian brain

Jun Kohyama[a], Takuro Kojima[b,c,d], Eriko Takatsuka[a], Toru Yamashita[b,c], Jun Namiki[b], Jenny Hsieh[e], Fred H. Gage[f], Masakazu Namihira[a], Hideyuki Okano[b], Kazunobu Sawamoto[c,d], and Kinichi Nakashima[a,1]

[a]Laboratory of Molecular Neuroscience, Graduate School of Biological Sciences, Nara Institute of Science and Technology, Nara 630-0101, Japan; [b]Department of Physiology, and [c]Bridgestone Laboratory of Developmental and Regenerative Neurobiology, Keio University School of Medicine, Tokyo 160-8582, Japan; [d]Department of Developmental and Regenerative Biology, Nagoya City University Graduate School of Medical Sciences, 1 Kawasumi, Mizuho-ku, Nagoya 467-8601, Japan; [e]Department of Molecular Biology and Cecil H. and Ida Green Center for Reproductive Biology Sciences, UT Southwestern Medical Center, Dallas, TX 75390; and [f]Laboratory of Genetics, The Salk Institute, La Jolla, CA 92037

Contributed by Fred H. Gage, October 2, 2008 (sent for review July 12, 2008)

Neural stem/progenitor cells (NSCs/NPCs) give rise to neurons, astrocytes, and oligodendrocytes. It has become apparent that intracellular epigenetic modification including DNA methylation, in concert with extracellular cues such as cytokine signaling, is deeply involved in fate specification of NSCs/NPCs by defining cell-type specific gene expression. However, it is still unclear how differentiated neural cells retain their specific attributes by repressing cellular properties characteristic of other lineages. In previous work we have shown that methyl-CpG binding protein transcriptional repressors (MBDs), which are expressed predominantly in neurons in the central nervous system, inhibit astrocyte-specific gene expression by binding to highly methylated regions of their target genes. Here we report that oligodendrocytes, which do not express MBDs, can transdifferentiate into astrocytes both *in vitro* (cytokine stimulation) and *in vivo* (ischemic injury) through the activation of the JAK/STAT signaling pathway. These findings suggest that differentiation plasticity in neural cells is regulated by cell-intrinsic epigenetic mechanisms in collaboration with ambient cell-extrinsic cues.

glia | JAK/STAT

The mammalian cerebral cortex originates from neural stem/neural progenitor cells (NSCs/NPCs), which self-renew and give rise to the three major brain cell types: neurons, astrocytes, and oligodendrocytes (1). The fate of NSCs/NPCs in the developing brain is believed to be determined by external cues that involve various types of cytokines and internal cellular programs (2, 3).

Among the three NSC/NPC progenies, astrocyte differentiation from NSCs/NPCs is largely dependent on the activation of the Janus kinase (JAK)/signal transducer and activator of transcription (STAT) pathway (4, 5). Impairment of astrocyte differentiation in gene knockout mice lacking leukemia inhibitory factor (LIF) (6), LIF receptor β (7), gp130 (8), and STAT3 (9) strongly suggests that the JAK-STAT signaling pathway plays a critical role for astrogliogenesis in the developing central nervous system (CNS).

Cell-intrinsic programs regulating fate determination of NSCs/NPCs include epigenetic modifications such as chromatin remodeling and DNA methylation. The cytosine residue in CpG dinucleotides of vertebrate genomes is a well-known target for DNA methylation, leading to suppression of methylated genes. Establishment of the proper gene methylation patterns is essential for inactivation of the X-chromosome, genomic imprinting, and normal development. Consistently, abnormalities in DNA methylation are associated with tumorigenesis (10) and with several neurological disorders including Rett (RTT), immunodeficiency-centromeric instability-facial anomalies (ICF), fragile-X, and α-thalassemia mental retardation (ATRX) syndromes (11).

Mechanistically, DNA methylation is considered to elicit its effects by interfering with binding of transcriptional factors to their cognate recognition sequences (12) or by creating a binding site for members of a transcriptional repressor family, the methyl-CpG binding proteins (MBDs), that recognize methylated CpG sequences (13).

During development, NSCs/NPCs change their differentiation potential via alternation of epigenetic modification. In early neurogenic period, the fetal NSCs/NPCs are unable to generate astrocytes even when stimulated with known astrocyte-inducing cytokines such as LIF, which activate the JAK/STAT pathway, due to DNA hypermethylation in the promoter regions of astrocytic genes (14, 15). The promoter regions become demethylated as gestation proceeds, conferring astrocyte differentiation potential to NSCs/NPCs in response to astrocyte-inducing cytokines. After CNS development is complete, differentiated cells may still be exposed to a variety of stimuli including physiological and pathological stress: for example, it has been reported that focal cerebral ischemia triggers JAK/STAT activation (16). Meanwhile, it remains unclear how differentiated cells maintain their traits or how their differentiation plasticity is regulated under normal or pathological conditions. There should at least be a mechanism of escaping from pathologic astrogliogenic stimuli on non astrocytic lineages.

In this study, we demonstrate that expression of MBDs is highly relevant to differentiation plasticity against astrocytic stimuli in adult neural cells. Oligodendrocytes which are devoid of MBDs can respond to JAK-STAT pathway activators and differentiate into astrocytes *in vitro*. Ectopic expression of MeCP2, one of the MBDs, in oligodendrocytes can suppress astrocytic differentiation even in the presence of astrocyte-inducing cytokines. By means of oligodendrocyte-fate tracing system, we further show that oligodendrocytes can convert into astrocytic lineages after brain ischemic injury. We thus provide a model in which *in vivo* unexpected cellular differentiation plasticity could contribute to the pathogenesis of injuries in the CNS.

Results

Oligodendrocytes but Not Neurons Have the Capacity to Respond to Astrogliogenic Stimulation. As a first step toward unraveling the mechanisms regulating the cellular identity of differentiated neural cells, we sought to examine whether neurons and oligodendrocytes express a typical astrocytic marker, glial fibrillary acidic protein (GFAP), in response to LIF stimulation. We used adult hippocampus-derived multipotent NPCs (AHPs) to obtain each differentiated cell type (17). When neurons were incubated with LIF for 2 days, no cells were found to be simultaneously positive for both the neuronal marker microtubule-associated protein 2ab (Map2ab) and GFAP (Fig. 1*A*, *Upper*). In this experiment, GFAP-positive cells were most likely to have differentiated from AHPs in response

Author contributions: J.K. and K.N. designed research; J.K., T.K., E.T., T.Y., J.N., and M.N. performed research; K.N. analyzed data; and J.K., J.H., F.H.G., H.O., K.S., and K.N. wrote the paper.

The authors declare no conflict of interest.

[1]To whom correspondence should be addressed. E-mail: kin@bs.naist.jp.

This article contains supporting information online at www.pnas.org/cgi/content/full/0808417105/DCSupplemental.

www.pnas.org/cgi/doi/10.1073/pnas.0808417105

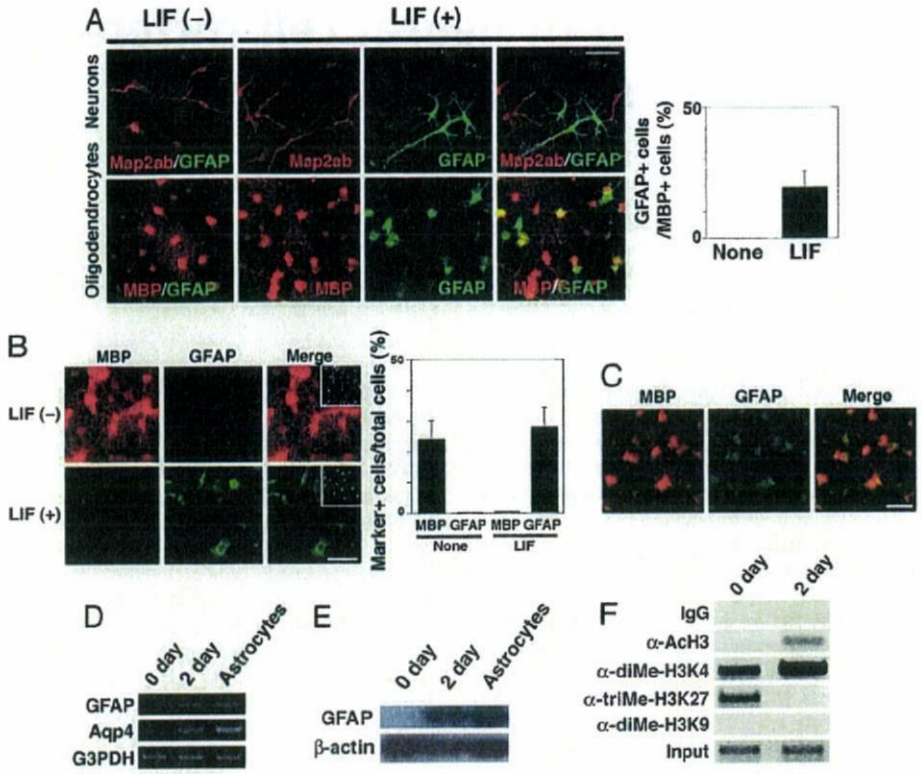

Fig. 1. Differentiation plasticity of oligodendrocytes. (*A*) AHP-derived neurons and oligodendrocytes were cultured for 2 days with or without LIF (50 ng/ml). Cells were then stained with sets of antibodies for Map2ab (*Upper*, red)/GFAP (*Upper*, green) and MBP (*Bottom*, red)/GFAP (*Lower*, green). (Scale bar: 50 μm.) The percentage of GFAP-positive cells in MBP-positive cells was quantified (*Right*). Data are mean ± SD. (*B*) Oligodendrocytes were cultured with or without LIF (50 ng/ml) for 4 days and subsequently stained for MBP (red) and GFAP (green). *Insets*: Hoechst nuclear staining of each field. (Scale bar: 50 μm.) Percentages of MBP- and GFAP-positive cells in total cells were quantified (*Right*). Data are mean ± SD. (*C*) GFAP-positive astrocytes appeared with LIF treatment for 2 days even when the cells were growth-arrested by aphidicolin (10 μg/ml). MBP (red), GFAP (green). (Scale bar: 50 μm.) (*D*) AHP-derived oligodendrocytes (0 day), oligodendrocytes incubated with LIF (50 ng/ml) for 2 days (2 day), and AHP-derived astrocytes were analyzed by RT-PCR using specific sets of primers against *gfap*, *Aqp4* and *G3PDH*. (*E*) AHP-derived oligodendrocytes (0 day), oligodendrocytes incubated with LIF (50 ng/ml) for 2 days (2 day), and AHP-derived astrocytes were analyzed by Western blot using an antibody against GFAP. A band corresponding to the molecular weight of GFAP protein (~50 kDa) was detected. (*F*) Differentiated oligodendrocytes (0 day) were incubated with LIF (50 ng/ml) for 2 days and then subjected to ChIP assay using control IgG, anti-diMe-H3K4, -diMe-H3K9, -triMe-H3K27 and -AcH3 antibodies. Co-immunoprecipitated *gfap* gene fragment (−18bp to + 513bp) was amplified by PCR with a specific set of primers. Nucleotide positions are those of GenBank accession number Z48978.

to LIF stimulation. In contrast, about 20% of cells that were positive for a mature oligodendrocyte marker, myelin basic protein (MBP), also became positive for GFAP in the LIF-stimulated condition, demonstrating their differentiation plasticity (Fig. 1*A*, *Lower* and *Right* graph). We also observed GFAP expression in a significant number of cells that were positive for another oligodendrocyte marker, CNPase [supporting information (SI) Fig. S1]. When we extended culturing with LIF to 4 days, MBP expression almost disappeared and the cells instead became exclusively GFAP-positive (Fig. 1*B*). We obtained similar results using a different astrocyte marker, S100β, with MBP (Fig. S2), and another oligodendrocyte marker, RIP, with GFAP (not shown). These results suggest that oligodendrocytes were converted into GFAP-positive astrocytes. GFAP expression in MBP-positive oligodendrocytes was observed, in the presence of LIF, even after treatment with the DNA polymerase inhibitor aphidicolin to arrest cell division (Fig. 1*C*). By measuring BrdU uptake, we confirmed that the cells were indeed growth-arrested (not shown), which suggests that cell division is dispensable for oligodendrocyte-astrocyte (O-A) conversion.

Oligodendrocyte-Astrocyte Conversion Is Accompanied by Epigenetic Modification Change. We next asked whether a change in chromatin modifications around the *gfap* transcription initiation site in oligodendrocytes occurred during the O-A transition. As shown in Fig. 1*D*, transcription of *gfap* and of another astrocytic marker, *aquaporin4* (Aqp4) (18), was upregulated, and immunoblot analysis (Fig. 1*E*) revealed that GFAP levels were also strikingly higher. Histone H3-lysine 4 (H3K4) methylation and H3 acetylation are consistent markers of transcriptionally active genes, whereas silent genes are marked by increased levels of H3K9 and H3K27 methylation (19). Chromatin immunoprecipitation (ChIP) experiments showed that H3K4 methylation and H3 acetylation increased during the O-A transition (Fig. 1*F*), in agreement with the immunocytochemical data, revealing that the chromatin status of *gfap* was altered toward the active state following LIF stimulation. We could not detect a distinct signal corresponding to H3K9 methylation, which may indicate that *gfap* transcription is poised but not actively suppressed in oligodendrocytes by H3K27 methylation (20). In support of this idea, H3K27 trimethylation on *gfap* was observed before LIF treatment (Fig. 1*F*, 0 day).

Oligodendrocytes Convert into Astrocytes *in Vivo* After Injury. Given that O-A transition was observed *in vitro* when oligodendrocytes were stimulated by astrocyte-inducing cytokine, we then asked whether O-A conversion also occurs *in vivo*. To this end, we specifically labeled oligodendrocytes *in vivo* and traced their fates with the Cre-loxP recombination system (Fig. 2*A* and *B*). We intercrossed two transgenic mouse lines: 1) MBP-Cre-tg (21), in

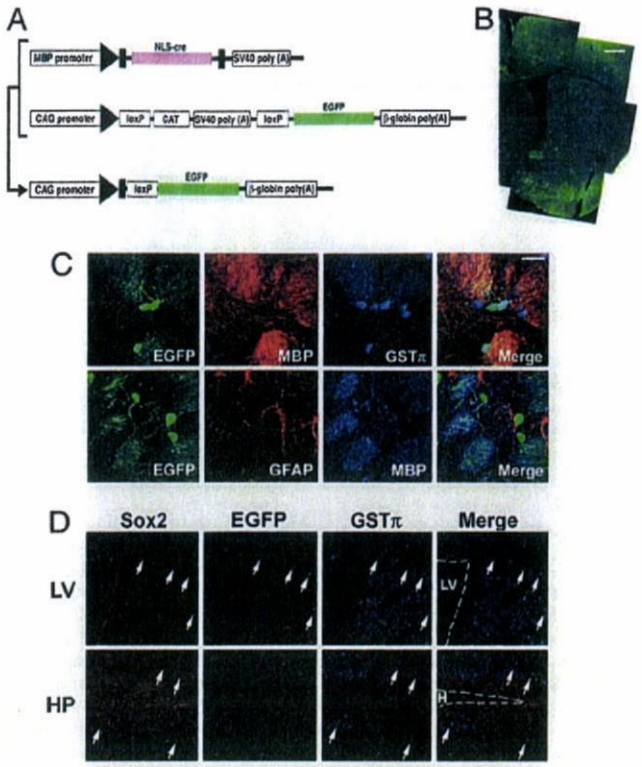

Fig. 2. Oligodendrocyte-specific labeling with EGFP. (*A*) Schematic of transgenic constructs used to trace the lineage of oligodendrocytes. In double-transgenic mice harboring the upper two transgenes, Cre recombinase is expressed in MBP-expressing oligodendrocytes and excises the floxed CAT-SV40 poly(A) fragment, resulting in constitutive expression of EGFP under the control of the ubiquitous CAG promoter. (*B*) Distribution of EGFP-positive cells in the adult brain. (Scale bar: 500 mm.) (*C*) EGFP expression was confined to MBP- and GST-π-positive mature oligodendrocytes in the adult brain under normal conditions (*Upper*). Expression of EGFP and GFAP was mutually exclusive (*Lower*). (Scale bar: 20 μm.) (*D*) Expression of EGFP in neurogenic regions of the adult brain. Arrows indicate representative cells expressing EGFP and the oligodendrocyte marker GST-π. Sox2 expression was not observed in the EGFP-positive cells. LV, lateral ventricle; HP, hippocampus; H, hilus. (Scale bar: 100 mm.)

which Cre recombinase is expressed under the control of the *mbp* promoter, and 2) CAG-CAT-EGFP-tg (22), in which EGFP expression is induced in Cre-expressing cells and their progeny under the control of the ubiquitous CAG promoter. Accordingly, in double-transgenic mice, once cells differentiate into MBP-expressing mature oligodendrocytes, they should sustain EGFP expression irrespective of what cell type they later become. We confirmed the previously determined specificity of the MBP promoter (21), and found that EGFP expression occurred exclusively in MBP-positive oligodendrocytes, but not in other cell types such as GFAP-positive astrocytes, in the adult brain of double-transgenic mice under normal conditions (Fig. 2*C*). The EGFP expression was not observed in a NSC/NPC marker Sox2-positive cells localized in the subventricular zone of the lateral ventricle or the subgranular zone of the hippocampus (Fig. 2*D*). EGFP was not expressed in cells positive for NG2, a marker for immature oligodendrocytes and/or glial progenitors (23) (data not shown). These results suggest that activation of the *mbp* promoter is confined to mature oligodendrocytes.

Because GFAP expression is dramatically induced by CNS injury (24), we subjected the double-transgenic mice to middle cerebral artery occlusion (MCAO) and traced the lineage of EGFP-positive cells. MCAO has been reported to activate the JAK/STAT pathway, as is the case with LIF stimulation (16). Consistent with the previous finding, we indeed detected STAT3 activation in oligodendrocytes after MCAO injury (Fig. 3*A*). Cells positive for both EGFP and phosphorylated STAT3 seemed to retain oligodendrocytic characteristics as judged by oligodendrocyte-specific marker expression 3 days after MCAO (Fig. 3*B*). Two weeks after surgery, we found that significant numbers of EGFP-positive cells became GFAP-positive astrocytes in and around the infarct area (Fig. 3 *C* and *D*), but not in unlesioned areas. Almost all other EGFP-positive/GFAP-negative cells still expressed MBP and appeared to retain oligodendrocytic characteristics (Fig. S3). We found no evidence for BrdU uptake in EGFP-positive cells after MCAO, probably because they did not divide during the O-A transition (Fig. S4). EGFP and GFAP double-positive cells were negative for cleaved caspase 3, indicating that they were not apoptotic (Fig. S5). Although one might argue that the *mbp* promoter was ectopically *trans*-activated in these GFAP-expressing astrocytes after injury, we could not detect EGFP expression in cultured astrocytes derived from adult MBP-cre/EGFP mice even when the cells were stimulated with LIF (Fig. 3*E*). Furthermore, the possibility that EGFP-positive cells de-differentiated into NSCs/NPCs is unlikely, because we could not detect ectopic or re-expression of the NSC/NPC neural marker Sox2 in these cells after injury (Fig. S6). Moreover, EGFP-positive cells also became GFAP-positive when the transgenic mice were subjected to another injury model, cold injury (Fig. S7), implying that the O-A transition occurs after diverse types of brain injury.

Neuron-Specific Expression of Methyl CpG Binding Proteins (MBDs) in CNS. Because epigenetic modification is known to be critically involved in defining cell-typespecific gene expression, we hypothesized that an epigenetic mechanism could be responsible for the differentiation plasticity of these neural cells. We therefore examined the DNA methylation status of *gfap* in each neural cell type derived from adult AHPs by the bisulfite sequencing method (Fig. 4*A*) and found that the *gfap* promoter region around the STAT3 binding site was completely unmethylated, whereas the region around the transcriptional start site was extensively methylated, in all of the neural cell types. Next, we examined the expression of MeCP2, a member of the MBD family, because we have recently reported that MBDs play an important role in restricting astrocyte-specific gene expression in neurons that have differentiated from fetal NPCs (25). Representative brain sections stained with antibodies against MeCP2 and against markers of neurons (NeuN), oligodendrocytes (GST-π) and astrocytes (S100β) are shown in Fig. 4 *B* and *C*. In oligodendrocyte fate-tracing mice, as mentioned above, MeCP2 expression was not observed in oligodendrocytes that were labeled by EGFP (Fig. 4*D*). These results are consistent with previous reports that MBDs are expressed predominantly in neurons, and not in glial cells, in the CNS (26). Neurons, but not oligodendrocytes or astrocytes, that have differentiated from AHPs *in vitro* also express MeCP2 (Fig. 4*E*). As has been observed for fetal NSCs/NPCs and cells differentiated from them (25), we found that in all neural cell types derived from AHPs the region around the *gfap* transcription initiation site was extensively methylated (Fig. 4*A*), suggesting that this region is a target for MBD binding in cells expressing MBDs (26) (Fig. 4*D*) to suppress *gfap* expression. Furthermore, we also found that another MBD, MBD1, shows a quite similar distribution to MeCP2 in adult brain (Fig. 4*F*).

MeCP2 Is Sufficient to Restrict Astrocytic Gene Expression. In light of the above findings, we examined the function of MeCP2 in terms of astrocytic differentiation of cells that are competent for LIF stimulation, i.e., NSCs/NPCs and oligodendrocytes. AHPs, which normally express GFAP in response to LIF, were transduced with recombinant retroviruses engineered to express EGFP (control) or both EGFP and MeCP2. In AHPs, the ectopic expression of MeCP2 led to suppression of astrocytic fate, consistent with our previous observation in fetal NSCs/NPCs (Fig. 5*A* and *B*). Next, to examine the possibility that the O-A conversion potential of oligo-

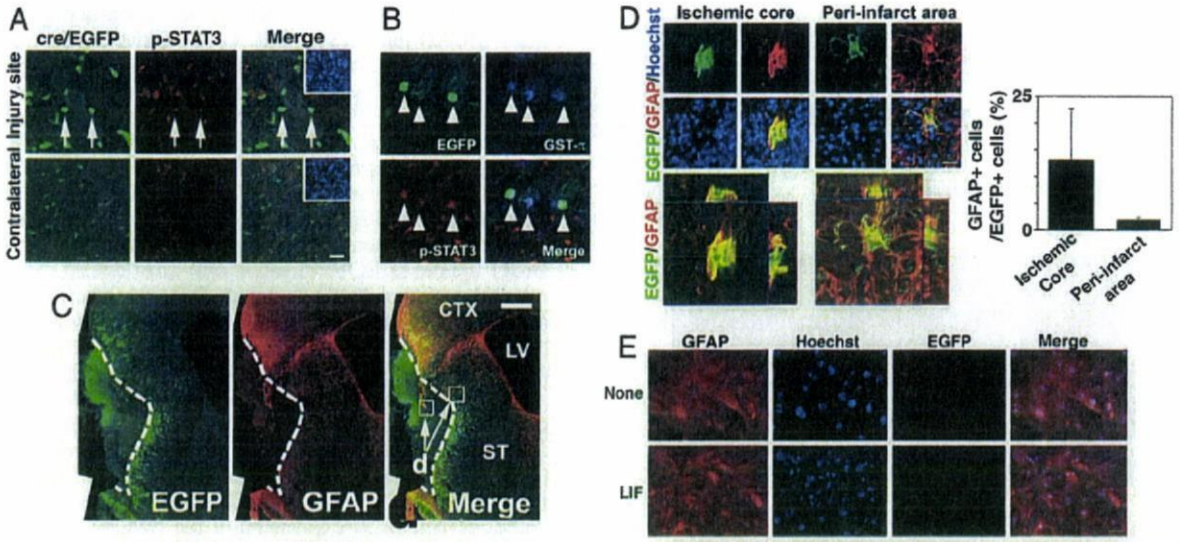

Fig. 3. STAT activation and O-A conversion after ischemic injury. (*A*) Activation of the JAK/STAT pathway in EGFP-positive cells was evaluated by immunostaining using an antibody against phospo-STAT3 (*p*-STAT3) in the injured and contralateral sides of the striata 72 h after ischemic injury. Arrows indicate representative cells positive for both EGFP and *p*-STAT3. (Scale bar: 20 μm.) *Insets*: Hoechst nuclear staining of each field. (*B*) *p*-STAT3 was also detected in GST*π*-expressing EGFP-positive cells 72 h after injury (arrowheads). (Scale bar: 20 μm.) (*C*) A representative brain section stained with anti-GFP and -GFAP antibodies 2 weeks after MCAO surgery. Scale bar = 500 μm. CTX, cortex; CC, corpus callosum; LV, lateral ventricle; ST, striatum. (*D*) Higher magnification views of square areas in *C*. GFAP expression appeared in EGFP-expressing cells in the ischemic core (*Left* square arrowed in *C*, *Upper Left*) and peri-infarct (*Right* square arrowed in *C*, *Upper Right*) areas. Representative cells positive for both GFAP and EGFP are shown; *Lower Right* image in each group is a superimposition of the other three images. (Scale bar: 20 μm.) Three-dimensional digital images of each area are also shown (ischemic core area, *Bottom Left*; peri-infarct area, *Bottom Right*). Percentage of GFAP-positive cells in EGFP-positive cells was quantified for each area (graph). Data are mean ± SD. (*E*) Astrocytes prepared from adult MBP-Cre/EGFP transgenic mice were left untreated or treated with LIF for 4 days, and then stained for EGFP (green) and GFAP (red). (Scale bar: 50 μm.) EGFP expression was not induced even when the cells were stimulated with LIF.

dendrocytes might be attributable to the lack of MBD expression, we transfected AHPs with MBP-Cre vector and control floxed neo or floxed neo-MeCP2-expressing vector together with floxed CAT-EGFP-expressing vector, and subsequently differentiated them into oligodendrocytes, then stimulated with LIF for 4 days. As shown in Fig. 5*C*, GFAP and S100β expression was clearly inhibited by the expression of MeCP2 in oligodendrocytes.

Discussion

It has become increasingly evident that a dynamic interplay between cellular extrinsic cues and cell intrinsic programs plays important roles in the fate determination of NSCs/NPCs. Among cell internal programs, epigenetic modification, especially DNA methylation, is important for acquisition of astrocyte-differentiation potential in NCSs/NPCs. In this work, we have shown that DNA methylation plays a critical role in restricting astrocytic property in neural cells in concert with MBDs. Notably, the astrocyte differentiation potential of oligodendrocytes may be attributable to loss of DNA methylation in the promoter regions of astrocytic genes and undetectable expression of MBDs. We have shown that oligodendrocytes derived from adult AHPs can respond to an astrocyte-inducing cytokine to become GFAP-positive astrocytes (Fig. 1). We further demonstrate that oligodendrocytes can also convert to GFAP-positive astrocytes after ischemic injury (Fig. 2), although because we have not examined functional maturation of the oligodendrocyte-derived astrocytes, this point will need to be addressed further in a future study.

Regarding cell plasticity, we have previously shown that even adult NSCs/NPCs retain substantial differentiation plasticity depending on the surrounding milieu (27). Ectopic expression of the proneural gene *ascl* (also known as *mash1*) induces oligodendrocyte differentiation of NSCs/NPCs located in one of the major neurogenic regions in the adult brain (the granular layer of the hippocampus), whereas it induces neuronal differentiation of NSCs/NPCs in another neurogenic region (the subventricular zone) and in *in vitro* culture conditions. Thus, it is becoming apparent that cells are more plastic than had previously been thought.

Our present study provides a molecular mechanism whereby cells can regulate their identity by repressing genes that are expressed in other lineages. Such an expression selectivity or exclusiveness of cell-type specific gene has been extensively examined in a series of studies of transcriptional repressor element1-silencing transcription factor (REST)/neuron-restrictive silencer factor (NRSF) (28). REST/NRSF suppresses neuronal gene expression in non-neural tissues to establish non-neuronal identity. Consistently REST/NRSF is expressed in non-neural tissues and dysfunction of REST/NRSF leads to ectopic neuronal gene expression in non-neural tissues. In contrast to the function of REST/NRSF, MBDs are expressed selectively in neurons in the CNS and repress glial genes (Figs. 4 and 5). We have previously shown by ChIP assay that MeCP2 binds to the highly methylated region of *gfap* in neurons that are expressing MeCP2 (25). MeCP2 deficiency in neurons may therefore lead to expression of genes that are normally astrocyte-specific. Indeed, many glial gene transcripts, including *gfap*, were found to be up-regulated in the brains of Rett syndrome patients with a mutation in *mecp2* (29). However, no major phenotype related to cellular differentiation in MeCP2-deficient mice is known, probably due to functional redundancy and overlapping expression among MBDs (25) (Fig. 4*F*). To address this point more precisely, we must await future studies in mice with compound disruption of several MBD genes.

It has long been thought that, after CNS injury, oligodendrocytes can only die, which could explain subsequent demyelination (30). However, we have shown here that significant numbers of oligodendrocytes actually become GFAP-positive cells following injury, suggesting that O-A conversion may be in part responsible for postinjury demyelination; oligodendrocytes may instead provide a source of newly generated GFAP-positive astrocytes in damaged nervous systems *in vivo*. Although astrocytes form a glial scar and are considered to be detrimental for axonal regeneration in the

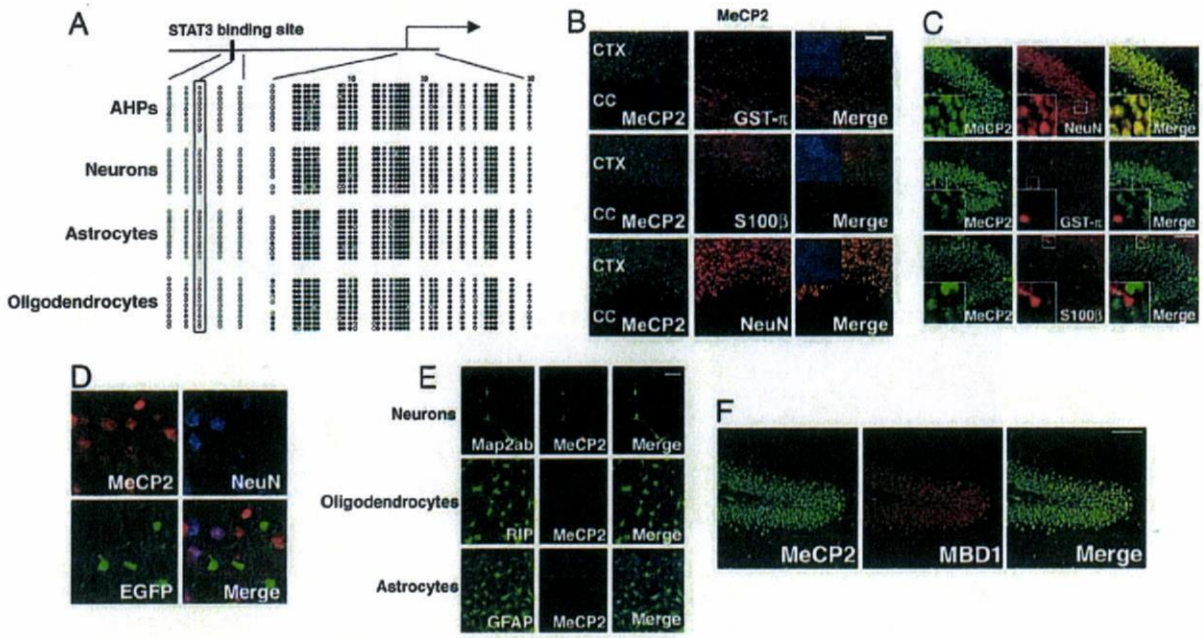

Fig. 4. MeCP2 is predominantly expressed in neurons and suppresses astrocytic gene expression in oligodendrocytes when ectopically expressed. (*A*) Schematic representation of *gfap* locus (*Upper*). Methylation status of five CpG sites around the STAT3 binding site (black box), which is critical for LIF-induced activation of the *gfap* promoter, and of 30 CpG sites around the transcription initiation site (arrow) were examined for each cell type by bisulfite sequencing. Open and closed circles indicate unmethylated and methylated CpG sites, respectively. (*B*) MeCP2 expression (green) was examined in adult mouse brain sections. Neurons, oligodendrocytes, and astrocytes are identified with specific antibodies for NeuN (red, *Upper* middle), GST-π (red, center), and S100β (red, *Lower* middle), respectively. Staining of the hippocampal dentate gyrus region is shown. *Insets*: higher magnification views of square areas in each field. (Scale bar: 50 μm.) (*C*) MeCP2 is predominantly expressed in neurons. MeCP2 expression (green) was examined in the adult mouse cortex and corpus callosum. Oligodendrocytes, astrocytes, and neurons were identified with specific antibodies for GST-π (red, *Upper* rows), S100β (red, middle rows), and NeuN (red, *Bottom* rows), respectively. *Insets*: Hoechst nuclear images of each field. (Scale bar: 100 μm.) CTX, cortex; CC, corpus callosum. (*D*) EGFP-positive cells do not express MeCP2. MeCP2 expression (*Upper Left*) was observed in NeuN-positive (*Upper Right*) but not in EGFP-positive (*Lower Left*) cells. (*E*) MeCP2 (red) is expressed in Map2ab-positive neurons (*Top*, green), but not in RIP-positive oligodendrocytes (middle, green) or GFAP-positive astrocytes (*Bottom*, green) generated from AHPs *in vitro*. (Scale bar: 50 μm.) (*F*) Redundant expression of MBDs *in vivo*. Expression of MeCP2 (green, *Left*) and MBD1 (red, middle), another member of the MBD family, was examined in the adult hippocampal region. These two MBDs showed the same expression pattern (*Right*). (Scale bar: 100 μm.)

injured CNS, it has been recently demonstrated that astrocytes also play a crucial role in wound healing and functional recovery in the subacute phase of spinal cord injury (31). During this phase, astrocytes migrate to compact the lesion, presumably excluding the inflammatory cells to prevent them from spreading in the parenchyma of the spinal cord. Assuming that astrocytes in the brain function as do those in the spinal cord, the oligodendrocyte-to-astrocyte conversion may contribute to an increase in the number of astrocytes after injury in the brain as well. We have also proposed an epigenetic mechanism to explain this differentiation plasticity of oligodendrocytes. To better understand how the injured brain might recover by shifting its cellular profile (e.g., from oligodendrocytes to astrocytes), this study emphasizes the need to consider both cell-intrinsic processes and cell-extrinsic cues. We suggest that epigenetic factors such as MBD proteins play important roles in the maintenance of cellular homeostasis after injury, providing a built-in system to relay signals from an ever-changing environment to the neural cell genome.

Materials and Methods

Cell Culture and *in Vitro* Differentiation. Neural progenitor cells (AHPs) isolated from hippocampus of adult female Fischer 344 rats, used in this study, have been characterized previously (32). The methods for maintaining AHPs and inducing their differentiation into specific lineages have been reported (17). For a detailed description, see *SI Text*.

Reverse TranscriptionPolymerase Chain Reaction. RNA isolation and reverse transcriptionpolymerase chain reaction (RT-PCR) were performed by an established method.

For a detailed description, see *SI Text*.

Western Blot Analysis. Western blot analysis was performed by an established method.

For a detailed description, see *SI Text*.

Immunostaining. Cells were fixed with 4% paraformaldehyde (PFA) and stained immunocytochemically, as described previously (25). For a detailed description, see *SI Text*.

Recombinant Retrovirus. Retrovirus was produced as previously described (33). For a detailed description, see *SI Text*.

Bisulfite Sequencing. Sodium bisulfite treatment of genomic DNA was performed essentially as described previously (34). For a detailed description, see *SI Text*.

Chromatin Immunoprecipitation Assay. Chromatin immunoprecipitation (ChIP) was performed according to a protocol published by Upstate Biotechnologies. AHP-derived oligodendrocytes and the cells cultured with LIF for 2 days were exposed to formaldehyde, at a final concentration of 1%, added directly to the tissue culture medium. Co-immunoprecipitated DNA was used as a template for PCR with the following set of primers: Gfex1S (5′-TGACATCCCAGGAGCCAG-3′) and Gfex1AS (5′-CAGTCTCTCTGCTCACTAGCC-3′).

Animals. MBP-Cre Tg mice (21) were provided by M. Miura (University of Tokyo, Japan). CAG-CAT-EGFP Tg mice (22) were a gift from J. Miyazaki (Osaka University, Japan). All experimental procedures and protocols were approved by the Animal Care and Use Committee of Keio University.

Focal Cerebral Ischemia. Mice were anesthetized by nitrous oxide/oxygen/isoflurane (69/30/1%) administered through an inhalation mask during surgery. Details of surgical procedures are provided in *SI Text*.

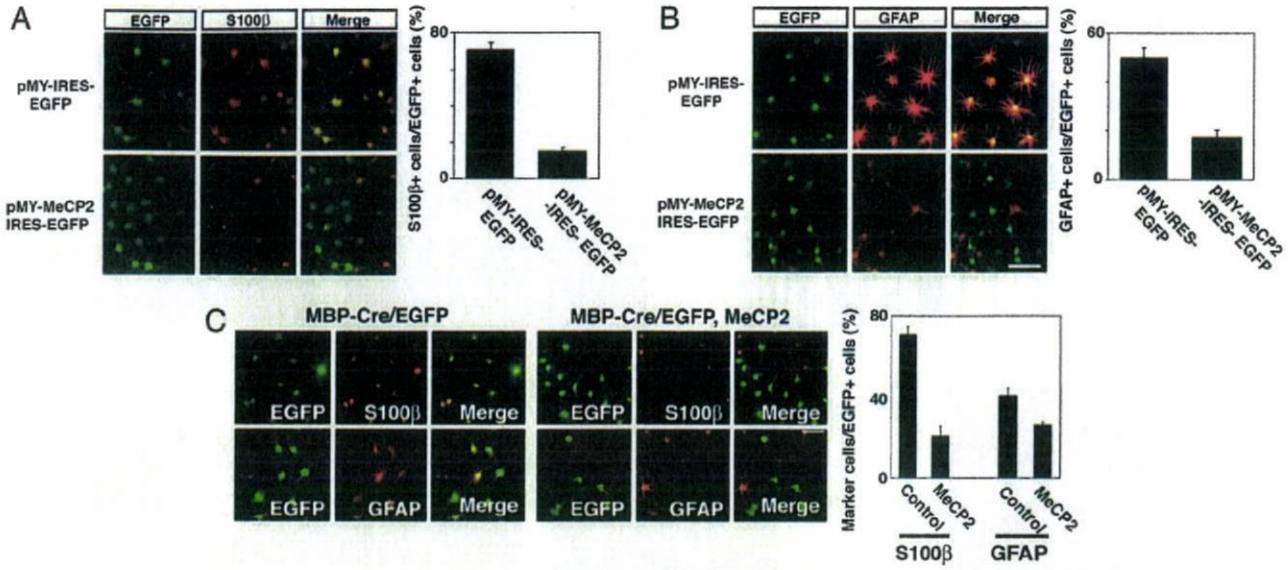

Fig. 5. MeCP2 expression is sufficient for inhibition of astrocyte differentiation of NSCs/NPCs and oligodendrocytes. (*A* and *B*) AHPs were infected with recombinant retrovirus engineered to express only EGFP (pMY), or MeCP2 together with EGFP (pMY-MeCP2-IRES-EGFP), cultured with LIF for 4 days and subjected to immunostaining. GFP (*A* and *B*, green), S100β (*A*, red), GFAP (*B*, red). (Scale bar: 50 μm.) Percentages of S100β- and GFAP-positive cells in EGFP-positive cells were quantified (*Upper* and *Lower* graphs, respectively). Data are mean ± SD. (*C*) AHPs were transfected with MBP-Cre together with CAG-CAT-EGFP and CAG floxed neo, or with CAG-CAT-EGFP and CAG floxed neo-MeCP2, and were allowed to differentiate into oligodendrocytes for 4 days. The cells were then cultured with LIF for an additional 4 days, followed by immunocytochemical staining using antibodies against GFAP and S100β. (Scale bar: 50 μm.) Percentages of GFAP- and S100β-positive cells in EGFP-expressing cells were quantified (*Right*). Data are mean ± SD.

ACKNOWLEDGMENTS. We thank Dr. M. Miura (University of Tokyo) for MBP-Cre transgenic mice, Dr. J. Miyazaki (Osaka University) for CAG-CAT-EGFP transgenic mice, Dr. T. Kitamura (University of Tokyo) for pMY vector and Plat-E cells, Dr. I. Saito (University of Tokyo) for pCALNL5 vector. We appreciate Drs. Y. Bessho and T. Matsui for valuable discussions. We also thank Drs. A. R. Muotri and I. Smith for helpful comments and critical reading of the manuscript. We are very grateful to N. Ueda for excellent secretarial assistance. Many thanks to N. Namihira, Y. Kuromi and K. Tsujimura for technical help. pCALNL5 was provided by RIKEN Brain Research Center, which is participating in the National Bio-Research Project of the Ministry of Education, Culture, Sports, Science and Technology, Japan. This work has been supported by a Grant-in-Aid for Young Scientists; a Grant-in-Aid for Science Research on Priority Areas; the Nara Institute of Science and Technology Global Centers of Excellence Program (Frontier Biosciences: Strategies for Survival and Adaptation in a Changing Global Environment) from the Ministry of Education, Culture, Sports, Science and Technology of Japan; and the Uehara Memorial Foundation.

1. Temple S (2001) The development of neural stem cells. *Nature* 414:112–117.
2. Gage FH (2000) Mammalian neural stem cells. *Science* 287:1433–1438.
3. Hsieh J, Gage FH (2004) Epigenetic control of neural stem cell fate. *Curr Opin Genet Dev* 14:461–469.
4. Bonni A, *et al.* (1997) Regulation of gliogenesis in the central nervous system by the JAK-STAT signaling pathway. *Science* 278:477–483.
5. Nakashima K, *et al.* (1999) Synergistic signaling in fetal brain by STAT3-Smad1 complex bridged by p300. *Science* 284:479–482.
6. Bugga L, Gadient RA, Kwan K, Stewart CL, Patterson PH (1998) Analysis of neuronal and glial phenotypes in brains of mice deficient in leukemia inhibitory factor. *J Neurobiol* 36:509–524.
7. Koblar SA, *et al.* (1998) Neural precursor differentiation into astrocytes requires signaling through the leukemia inhibitory factor receptor. *Proc Natl Acad Sci USA* 95:3178–3181.
8. Nakashima K, *et al.* (1999) Developmental requirement of gp130 signaling in neuronal survival and astrocyte differentiation. *J Neurosci* 19:5429–5434.
9. He F, *et al.* (2005) A positive autoregulatory loop of Jak-STAT signaling controls the onset of astrogliogenesis. *Nat Neurosci* 8:616–625.
10. Jones PA, Baylin SB (2002) The fundamental role of epigenetic events in cancer. *Nat Rev Genet* 3:415–428.
11. Robertson KD, Wolffe AP (2000) DNA methylation in health and disease. *Nat Rev Genet* 1:11–19.
12. Watt F, Molloy PL (1988) Cytosine methylation prevents binding to DNA of a HeLa cell transcription factor required for optimal expression of the adenovirus major late promoter. *Genes Dev* 2:1136–1143.
13. Hendrich B, Bird A (1998) Identification and characterization of a family of mammalian methyl-CpG binding proteins. *Mol Cell Biol* 18:6538–6547.
14. Takizawa T, *et al.* (2001) DNA methylation is a critical cell-intrinsic determinant of astrocyte differentiation in the fetal brain. *Dev Cell* 1:749–758.
15. Fan G, *et al.* (2005) DNA methylation controls the timing of astrogliogenesis through regulation of JAK-STAT signaling. *Development* 132:3345–3356.
16. Suzuki S, *et al.* (2001) Phosphorylation of signal transducer and activator of transcription-3 (Stat3) after focal cerebral ischemia in rats. *Exp Neurol* 170:63–71.
17. Hsieh J, *et al.* (2004) IGF-I instructs multipotent adult neural progenitor cells to become oligodendrocytes. *J Cell Biol* 164:111–122.
18. Shi Y, *et al.* (2004) Expression and function of orphan nuclear receptor TLX in adult neural stem cells. *Nature* 427:78–83.
19. Jenuwein T, Allis CD (2001) Translating the histone code. *Science* 293:1074–1080.
20. Bernstein BE, *et al.* (2006) A bivalent chromatin structure marks key developmental genes in embryonic stem cells. *Cell* 125:315–326.
21. Hisahara S, *et al.* (2000) Targeted expression of baculovirus p35 caspase inhibitor in oligodendrocytes protects mice against autoimmune-mediated demyelination. *EMBO J* 19:341–348.
22. Kawamoto S, *et al.* (2000) A novel reporter mouse strain that expresses enhanced green fluorescent protein upon Cre-mediated recombination. *FEBS Lett* 470:263–268.
23. Levine JM, Reynolds R, Fawcett JW (2001) The oligodendrocyte precursor cell in health and disease. *Trends Neurosci* 24:39–47.
24. Sofroniew MV (2005) Reactive astrocytes in neural repair and protection. *Neuroscientist* 11:400–407.
25. Setoguchi H, *et al.* (2006) Methyl-CpG binding proteins are involved in restricting differentiation plasticity in neurons. *J Neurosci Res* 84:969–979.
26. Jung BP, Zhang G, Ho W, Francis J, Eubanks JH (2002) Transient forebrain ischemia alters the mRNA expression of methyl DNA-binding factors in the adult rat hippocampus. *Neuroscience* 115:515–524.
27. Jessberger S, Toni N, Clemenson GD, Jr, Ray J, Gage FH (2008) Directed differentiation of hippocampal stem/progenitor cells in the adult brain. *Nat Neurosci* 11:888–893.
28. Ballas N, Mandel G (2005) The many faces of REST oversee epigenetic programming of neuronal genes. *Curr Opin Neurobiol* 15:500–506.
29. Colantuoni C, *et al.* (2001) Gene expression profiling in postmortem Rett Syndrome brain: Differential gene expression and patient classification. *Neurobiol Dis* 8:847–865.
30. Lyons SA, Kettenmann H (1998) Oligodendrocytes and microglia are selectively vulnerable to combined hypoxia and hypoglycemia injury in vitro. *J Cereb Blood Flow Metab* 18:521–530.
31. Okada S, *et al.* (2006) Conditional ablation of Stat3 or Socs3 discloses a dual role for reactive astrocytes after spinal cord injury. *Nat Med* 12:829–834.
32. Gage FH, *et al.* (1995) Survival and differentiation of adult neuronal progenitor cells transplanted to the adult brain. *Proc Natl Acad Sci USA* 92:11879–11883.
33. Morita S, Kojima T, Kitamura T (2000) Plat-E: An efficient and stable system for transient packaging of retroviruses. *Gene Ther* 7:1063–1066.
34. Clark SJ, Harrison J, Paul CL, Frommer M (1994) High sensitivity mapping of methylated cytosines. *Nucleic Acids Res* 22:2990–2997.

Neuroscience 155 (2008) 780–788

IDENTIFICATION OF GENES THAT RESTRICT ASTROCYTE DIFFERENTIATION OF MIDGESTATIONAL NEURAL PRECURSOR CELLS

T. SANOSAKA,[a] M. NAMIHIRA,[a] H. ASANO,[a] J. KOHYAMA,[a] K. AISAKI,[b] K. IGARASHI,[b] J. KANNO[b] AND K. NAKASHIMA[a]*

[a]*Laboratory of Molecular Neuroscience, Graduate School of Biological Sciences, Nara Institute of Science and Technology, 8916-5, Takayama, Ikoma, Nara 630-0101, Japan*

[b]*Division of Cellular and Molecular Toxicology, Biological Safety Research Center, National Institutes of Health Sciences, 1-18-1, Kamiyoga, Setagaya-ku, Tokyo 158-8501, Japan*

Abstract—During development of the mammalian CNS, neurons and glial cells (astrocytes and oligodendrocytes) are generated from common neural precursor cells (NPCs). However, neurogenesis precedes gliogenesis, which normally commences at later stages of fetal telencephalic development. Astrocyte differentiation of mouse NPCs at embryonic day (E) 14.5 (relatively late gestation) is induced by activation of the transcription factor signal transducer and activator of transcription (STAT) 3, whereas at E11.5 (mid-gestation) NPCs do not differentiate into astrocytes even when stimulated by STAT3-activating cytokines such as leukemia inhibitory factor (LIF). This can be explained in part by the fact that astrocyte-specific gene promoters are highly methylated in NPCs at E11.5, but other mechanisms are also likely to play a role. We therefore sought to identify genes involved in the inhibition of astrocyte differentiation of NPCs at midgestation. We first examined gene expression profiles in E11.5 and E14.5 NPCs, using Affymetrix GeneChip analysis, applying the Percellome method to normalize gene expression level. We then conducted *in situ* hybridization analysis for selected genes found to be highly expressed in NPCs at midgestation. Among these genes, we found that *N-myc* and high mobility group AT-hook 2 (*Hmga2*) were highly expressed in the E11.5 but not the E14.5 ventricular zone of mouse brain, where NPCs reside. Transduction of *N-myc* and *Hmga2* by retroviruses into E14.5 NPCs, which normally differentiate into astrocytes in response to LIF, resulted in suppression of astrocyte differentiation. However, sustained expression of *N-myc* and *Hmga2* in E11.5 NPCs failed to maintain the hypermethylated status of an astrocyte-specific gene promoter. Taken together, our data suggest that astrocyte differentiation of NPCs is regulated not only by DNA methylation but also by genes whose expression is controlled spatio-temporally during brain development.

*Corresponding author. Tel: +81-743-72-5471; fax: +81-743-72-5479.
E-mail address: kin@bs.naist.jp (K. Nakashima).

Abbreviations: bHLH, basic helix–loop–helix; BMP, bone morphogenetic protein; CNTF, ciliary neurotrophic factor; CT-1, cardiotrophin-1; DIG, digoxigenin; E, embryonic day; Gapdh, glyceraldehyde-3-phosphate dehydrogenase; GEO, Gene Expression Omnibus; *gfap*, glial fibrillary acidic protein; *Hmga2*, high mobility group AT-hook 2; JAK, janus kinase; LIF, leukemia inhibitory factor; NPC, neural precursor cell; SSC, sodium chloride sodium citrate; STAT, signal transducer and activator of transcription.

Key words: *N-myc*, *Hmga2*, epigenetics, Percellome method, differentiation.

The mammalian CNS is composed of neurons, astrocytes, and oligodendrocytes. Although these three cell types are derived from common multipotent neural precursor cells (NPCs), their differentiation is spatially and temporally regulated during development (Temple, 2001). Fetal telencephalic NPCs divide symmetrically in early gestation to increase their own numbers, and then undergo neurogenesis through mostly asymmetric divisions. Toward the end of the neurogenic phase, NPCs acquire multipotentiality to generate astrocytes and oligodendrocytes as well as neurons. It has recently become apparent that NPC fate determination is controlled by both extracellular cues, including cytokine signaling, and intracellular programs such as epigenetic gene regulation (Edlund and Jessell, 1999; Takizawa et al., 2001; Hsieh and Gage, 2004).

Interleukin (IL) -6 family cytokines such as cardiotrophin-1 (CT-1), leukemia inhibitory factor (LIF) and ciliary neurotrophic factor (CNTF) activate the janus kinase (JAK) –signal transducer and activator of transcription (STAT) signaling pathway and are known to induce astrocyte differentiation of NPCs (Bonni et al., 1997; Rajan and McKay, 1998). Gene knockouts of LIF (Bugga et al., 1998), LIF receptor β (Koblar et al., 1998), the common receptor component gp130 (Nakashima et al., 1999a) and STAT3 (He et al., 2005) all result in impaired astrocyte differentiation *in vivo*, emphasizing the contribution of JAK-STAT signaling to astrogliogenesis in the developing CNS. Bone morphogenetic proteins (BMPs) are another group of astrocyte-inducing cytokines. They synergistically induce astrocytic differentiation of NPCs via formation of a complex between STATs and BMP-activated transcription factor Smads, bridged by the transcriptional coactivators p300/CBP (Nakashima et al., 1999b).

In addition to these extracellular factors, intracellular programs and factors also play critical roles to regulate astrocytic differentiation of NPCs. We have previously shown that a CpG dinucleotide within a STAT3-binding element (TTC*CG*AGAA) in the astrocytic marker glial fibrillary acidic protein (*gfap*) gene promoter is highly methylated in NPCs at midgestation (embryonic day (E)11.5), when the cells differentiate only into neurons but not into astrocytes. Since STAT3 does not bind to the methylated cognate sequence, NPCs at midgestation do not express *gfap* even when stimulated by STAT3-activating cytokines such as LIF. As gestation proceeds, the STAT3-binding

0306-4522/08$32.00+0.00
doi:10.1016/j.neuroscience.2008.06.039

site becomes gradually demethylated in NPCs, enabling them to express *gfap* in response to LIF stimulation (Takizawa et al., 2001). Thus, we have proposed that DNA methylation is a critical cell-intrinsic determinant of astrocyte differentiation during brain development. However, the important question of how this astrocyte-specific gene promoter becomes demethylated in NPCs remains unanswered.

Neurogenic basic helix–loop–helix (bHLH) transcription factors have been also shown to regulate astrocyte differentiation during early neural development. Mice carrying mutations in *mash1* and *math3* (Tomita et al., 2000), or, to a lesser extent, *mash1* and *ngn2* (Nieto et al., 2001) exhibit decreased neurogenesis and premature astrogliogenesis. Conversely, overexpression of neurogenic bHLH factors, either *in vivo* during the gliogenic period (Cai et al., 2000) or in cultured NPCs exposed to CNTF (Sun et al., 2001), promotes neurogenesis at the expense of astrogliogenesis. A possible mechanism underlying the repressive effect on astrogliogenesis is that Ngn1 binds to p300/CBP and sequesters them away from STAT3, thereby preventing STAT3 from activating astrocytic gene expression (Sun et al., 2001). Such a mechanism may ensure the restriction of astrocyte differentiation in NPCs that would otherwise differentiate into neurons under the influence of high-level neurogenic bHLH factor expression during the neurogenic period.

Although these studies have provided us with an integrated insight into the mechanism of neurogenic-to-gliogenic switching in NPCs, they do not preclude the involvement of other, as yet unknown, factors. To identify such factors, we first in this study examined gene expression profiles of mid- and late-gestational NPCs by Affymetrix GeneChip analysis, which is widely used to obtain a complete picture of developmental stage-specific gene expression (Abramova et al., 2005; Ajioka et al., 2006). We then performed *in situ* hybridization experiments to investigate the spatio-temporal expression pattern of genes that were found to be highly expressed in midgestational NPCs. Two genes, *N-myc* and high mobility group AT-hook 2 (*Hmga2*), were highly expressed in the ventricular zone of E11.5 but not of E14.5 mouse brain. Transduction of *N-myc* and *Hmga2* into E14.5 NPCs resulted in suppression of astrocyte differentiation, even in the presence of LIF. However, the prolonged expression of these genes in E11.5 NPCs failed to preserve the hypermethylated status of the astrocyte-specific *gfap* promoter. These results suggest that the inhibition of astrocyte differentiation in midgestational NPCs is regulated not only by DNA methylation of astrocyte-specific gene promoters but also by transcription-regulating factors whose expression is controlled spatiotemporally during brain development.

EXPERIMENTAL PROCEDURES

NPC culture

Timed-pregnant ICR mice were used to prepare NPCs. The protocols described below were carried out according to the animal experimentation guidelines of Nara Instititute of Science and Technology that comply with National Institutes of Health Guide for Care and Use of Laboratory Animals. All efforts were made to minimize the number of animals used and their suffering. NPCs were prepared from telencephalons of E11.5 and E14.5 mice and cultured as described previously (Nakashima et al., 1999b). Briefly, the telencephalons were triturated in Hanks' balanced salt solution by mild pipetting with a 1-ml pipet tip (Gilson, Middleton, WI, USA). Dissociated cells were cultured in N2-supplemented Dulbecco's Modified Eagle's Medium with F12 (GIBCO, Grand Island, NY, USA) containing 10 ng/ml basic FGF (R&D Systems, Minneapolis, MN, USA) (N2/DMEM/F12/bFGF) on culture dishes (Nunc, Naperville, IL, USA) or chamber slides (Nunc) which had been precoated with poly-L-ornithine (Sigma, St. Louis, MO, USA) and fibronectin (Sigma).

Immunocytochemistry

E11.5 and E14.5 NPCs cultured on coated chamber slides were washed with PBS, fixed in 4% paraformaldehyde in PBS, and stained with the following primary antibodies: rabbit anti-SOX2 (1:1000, Chemicon, Temecula, CA, USA), mouse anti-βIII-tubulin (1:500, Sigma), rabbit anti-GFAP (1:2000, Dako, High Wycombe, UK). The following secondary antibodies were used: Alexa488-conjugated goat anti-rabbit IgG (1:500, Molecular Probes, Eugene, OR, USA), Cy3-conjugated goat anti-mouse IgG (1:500, Chemicon). Nuclei were stained using bisbenzimide H33258 fluorochrome trihydrochloride (Nacalai Tesque, Kyoto, Japan). All experiments were independently replicated at least three times.

Sample preparation and GeneChip analysis

These procedures were conducted according to the Percellome method (Kanno et al., 2006) to normalize mRNA expression values to sample cell numbers by adding external spike mRNAs to the sample in proportion to the genomic DNA concentration and utilizing the spike RNA quantity data as a dose-response standard curve for each sample. Cells cultured on coated dishes were washed with PBS, lysed in 500 ml of RLT buffer (Qiagen K.K., Tokyo, Japan) and transferred to a 1.5-ml tube. Two separate 10-μl aliquots were treated with DNAse-free RNase A (Nippon Gene, Tokyo, Japan) for 30 min at 37 °C, followed by proteinase K (Roche Diagnostics, Mannheim, Germany) for 3 h at 55 °C, and then transferred to a 96-well black plate. PicoGreen fluorescent dye (Molecular Probes) was added to each well, and then incubated for 2 min at 30 °C. The DNA concentration was measured using a 96-well fluorescence plate reader with excitation at 485 nm and emission at 538 nm. Lamda phage DNA (PicoGreen kit, Molecular Probes) was used as standard. The appropriate amount of spike RNA cocktail was added to the sample homogenates in proportion to their DNA concentration. Five independent *Bacillus subtilis* poly-A RNAs were included in the grade-dosed spike cocktail. Total RNAs were purified using an RNeasy Mini kit (Qiagen), according to the manufacturer's instructions. First-strand cDNAs were synthesized by incubating 5 μg of total RNA with 200 U SuperScript II reverse transcriptase (Invitrogen, Carlsbad, CA, USA) and 100 pmol T7-$(dT)_{24}$ primer [5′-GGCCAG-TGAATTGTAATACGACTCACTATAGGGAGGCGG-$(dT)_{24}$-3′]. After second-strand synthesis, the double-stranded cDNAs were purified using a GeneChip Sample Cleanup Module (Affymetrix, Washington, DC, USA), according to the manufacturer's instructions, and labeled by *in vitro* transcription using a BioArray HighYield RNA transcript labeling kit (Enzo Life Sciences, Farmingdale, NY, USA). The labeled cRNA was then purified using a GeneChip Sample Cleanup Module (Affymetrix) and treated with fragmentation buffer at 94 °C for 35 min. For hybridization to a GeneChip Mouse Genome 430 2.0 Array (Affymetrix), 15 μg of fragmented cRNA probe was incubated with 50 pM control oligonucleotide B2, 1× eukaryotic hybridization control (1.5 pM BioB, 5 pM BioC, 25 pM BioD and 100 pM Cre), 0.1 mg/ml herring sperm

DNA, 0.5 mg/ml acetylated BSA and 1× manufacturer-recommended hybridization buffer in a 45 °C rotisserie oven for 16 h. Washing and staining were performed in a GeneChip Fluidics Station (Affymetrix) using the appropriate antibody amplification, washing and staining protocols. The phycoerythrin-stained arrays were scanned as digital image files, which were analyzed with GeneChip Operating Software (Affymetrix). The expression data were converted to copy numbers of mRNA per cell by the Percellome method, quality controlled, and analyzed using Percellome software (Kanno et al., 2006). The GeneChip data have been deposited in the NCBI Gene Expression Omnibus (GEO; http://www.ncbi.nlm.nih.gov/geo/) and is accessible through GEO series accession number GSE 10796.

Quantitative real-time RT-PCR

Quantitative real-time PCR was performed to confirm the results of GeneChip analysis. RNAs from E11.5 and E14.5 NPCs were reverse transcribed using Superscript II (Invitrogen) and amplified by PCR, with a specific pair of primers for each gene, using the Mx3000P system (Stratagene, La Jolla, CA, USA). The expression of target genes was normalized to that of glyceraldehyde-3-phosphate dehydrogenase (*Gapdh*). The gene-specific primers were as follows: mouse N-myc: N-myc-S, 5′-aactatgctgcaccctcacc-3′; N-myc-AS, 5′-tagcaagtccgagcgtgttc-3′; mouse Hmga2: Hmga2-S, 5′-ggcagccgtccacatcag-3′; Hmga2-AS, 5′-taatcctcctctgcggactc-3′; mouse Sox11: Sox11-S, 5′-gagcctgtacgacgaagtgc-3′; Sox11-AS, 5′-tgaacaccaggtcggagaag-3′; mouse Bhlhb5: Bhlhb5-S, 5′-gttgcgcctcaacatcaac-3′; Bhlhb5-AS, 5′-acttttgcagaggctggac-3′; mouse Bcl11a: Bcl11a-S, 5′-gcatcaagctggagaaggag-3′; Bcl11a-AS, 5′-gagcttccatccgaaaactg-3′; mouse Gapdh: Gapdh-S, 5′-accacagtccatgccatcac-3′; Gapdh-AS, 5′-tccaccaccctgttgctgta-3′.

In situ hybridization

Digoxigenin- (DIG; Roche) labeled cRNA probes were synthesized for each gene, following the manufacturer's instructions. Cryosections were washed with PBS and fixed with 4% PFA. After fixation, sections were incubated in prehybridization solution (5× sodium chloride sodium citrate (SSC), 1% SDS, 50 μg/ml yeast transfer RNA, 50 μg/ml heparin in 50% formamide) at 70 °C for 1 h and hybridized with 500 ng/ml of DIG-labeled cRNA probes at 65 °C for 16 h. After three washes with wash solution 1 (5× SSC, 1% SDS in 50% formamide) and wash solution 3 (2× SSC in 50% formamide), sections were blocked with 10% normal sheep serum in TBST at room temperature for 1 h and then incubated with 1:1000 alkaline phosphatase-conjugated anti-DIG antibody (Roche) at 4 °C for 16 h. After four washes with TBST, hybridized probes were visualized with 5-bromo-4-chloro-3 indolylphosphate and nitro blue tetrazolium chloride.

Recombinant retrovirus construction and infection

Human *N-myc* and mouse *Hmga2* cDNAs were cloned into the expression vector pMYs, which contains an internal ribosome entry site followed by the region upstream of the *EGFP* gene (Morita et al., 2000). The Plat-E packaging cell line was transiently transfected with the retrovirus DNA by Trans-IT 293 (Mirus, Madison, WI, USA) (Morita et al., 2000). On the following day, the medium was replaced with N2/DMEM/F12/bFGF, and the cells were cultured in this medium for 1 day before virus was collected.

Fluorescence activated cell sorting

Virus-infected E11.5 NPCs were cultured for 4 days, after which GFP-labeled cells were sorted using a FACS Vantage (Becton Dickinson, Franklin Lakes, NJ, USA) at a flow rate of less than 1500 events/s; gating parameters were set by side and forward scatter to eliminate debris, dead and aggregated cells. After sorting, genomic DNA was extracted and used for bisulfite sequencing.

Bisulfite sequencing

Sodium bisulfite treatment of genomic DNA was performed using a Methylamp DNA Modification kit (Epigentek, Brooklyn, NY, USA), according to the manufacturer's instructions. The region in the *gfap* promoter containing the STAT-binding site of the bisulfite-treated genomic DNA was amplified by PCR using the following primers: GFmS (5′-GGGATTTATTAGGAGAATTTTAGAAGTAG-3′), GFmAS (5′-TCTACCCATACTTAAACTTCTAATATCTAC-3′). The PCR products were cloned into pT7Blue vector (Novagen, Madison, WI, USA) and at least 12 randomly selected clones were sequenced.

RESULTS

Preparation of NPCs from different developmental stages and comparison of their gene expression profiles by GeneChip analysis

E11.5 NPCs do not differentiate into astrocytes, even in the presence of the astrocyte-inducing cytokine LIF, in contrast to 4-day cultured E14.5 NPCs (Takizawa et al., 2001). As a first step toward identifying factors involved in the inhibition of astrocyte differentiation of NPCs at midgestation, we examined the gene expression profiles of E11.5 and E14.5 NPCs.

E11.5 and E14.5 NPCs were isolated from embryonic telencephalon and cultured as indicated in Fig. 1A. To evaluate the purity of NPCs in each cell population, the cells were stained with antibody against SOX2, an NPC marker (Graham et al., 2003). As shown in Fig. 1B and C, the majority of cells in both populations were positive for SOX2, indicating that NPCs were highly enriched. An Affymetrix mouse genome GeneChip array was chosen to compare expression profiles in the two populations, and we adopted the Percellome method to normalize gene expression from different samples (Kanno et al., 2006). The method enabled us to quantify mRNA molecules per cell based on the measurement of cell by adding a grade-dosed spike cocktail to the samples. We excluded genes whose transcript copy number was below six per cell. Scatter plots illustrating the differences between E11.5 and E14.5 NPCs are shown in Fig. 1D; 194 genes were expressed at >fivefold higher level in E11.5 NPCs than in E14.5 NPCs (Fig. 1D, light blue zone). Of these, 102 were known genes, and were classified by functional category (Fig. 1E). Since we wished to identify negative regulators of astrocyte differentiation, or factors involved in the epigenetic modification in midgestational NPCs, we focused on transcription-related genes (Fig. 1E, red). These 21 genes are listed in Table 1, and five (*N-myc*, *Hmga2*, *Bhlhb5*, *Sox11*, *Bcl11a*) were selected for further analysis because they have been reported to play roles in cell growth, differentiation, and chromatin remodeling in other types of stem cells (Sawai et al., 1990; Zhou et al., 1995; Saiki et al., 2000; Knoepfler et al., 2002; Brunelli et al., 2003; Sock et al., 2004).

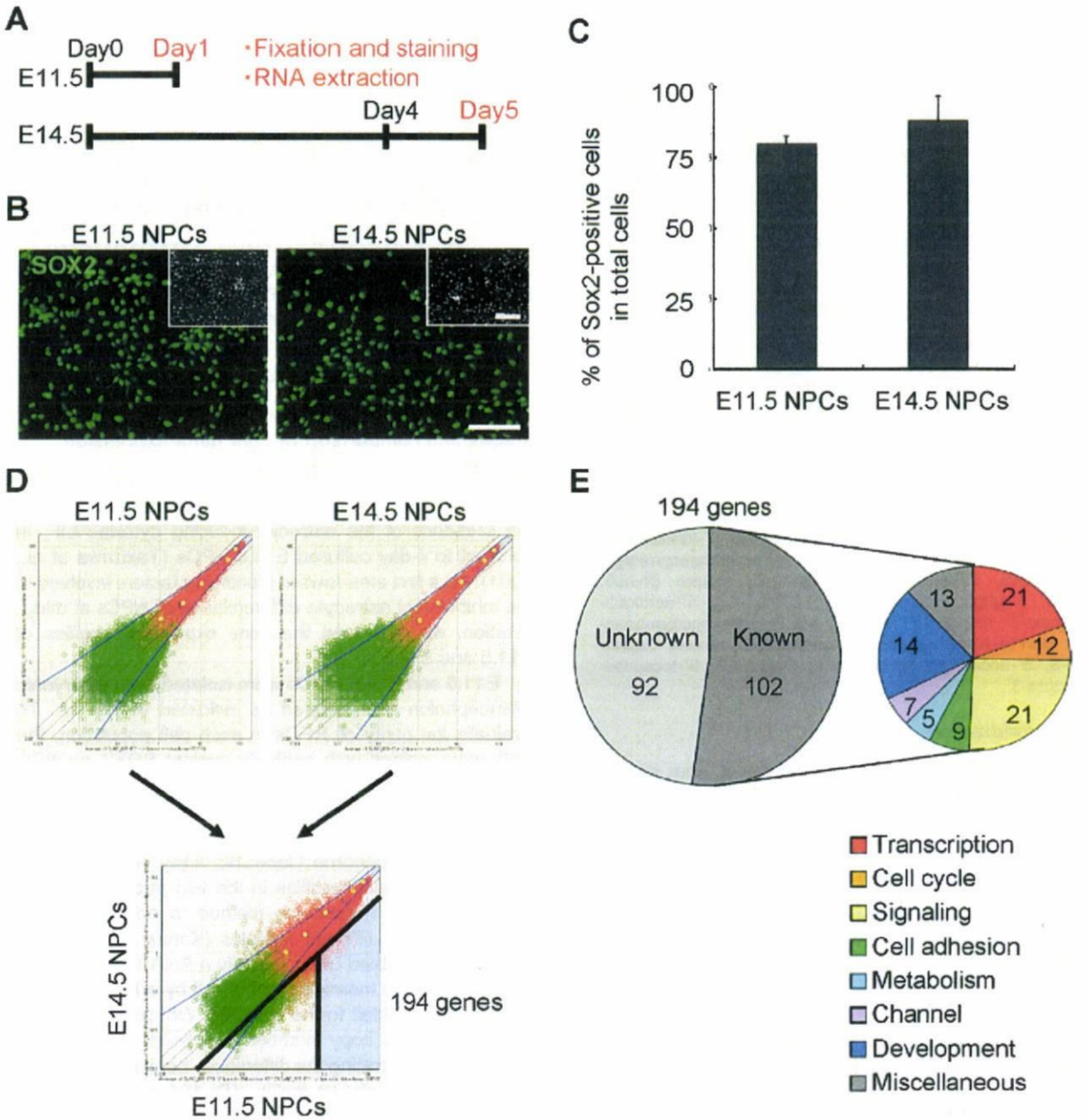

Fig. 1. Comparison of gene expression profiles in E11.5 and E14.5 NPCs. (A) Schematic of experimental protocol. NPCs isolated from E11.5 mouse telencephalon were plated (day 0) and used on the following day for immunostaining and RNA extraction (day 1). NPCs isolated at E14.5 were expanded for 4 days and replated on day 4. On day 5, these cells were fixed for immunostaining. RNA was also extracted. (B) E11.5 and E14.5 NPCs were stained with antibody against Sox2 (green). Scale bar=25 μm. Insets: Hoechst nuclear staining of each field. Scale bar=25 μm. (C) The percentage of Sox2-positive cells in E11.5 and E14.5 NPCs was quantified. Mean±S.D. (D) Scatter plots of E11.5 (upper left) and E14.5 (upper right) samples obtained from GeneChip analysis indicated no significant change between independent experiments with the same sample. Overview (lower plot) of gene expression change was compared between each sample. One hundred ninety-four genes were expressed at >fivefold higher level in E11.5 NPCs than E14.5 NPCs (light blue zone). (E) Of the 194 genes that were highly expressed in E11.5 NPCs, known genes were classified according to Affymetrix gene ontology. For interpretation of the references to color in this figure legend, the reader is referred to the Web version of this article.

Table 1. Transcription-related genes highly expressed in E11.5 NPCs

Probe set ID	GenBank ID	Gene symbol	E11.5 NPCs	E14.5 NPCs	E11.5/ E14.5
1433919_at	AV302111	*Asb4*	9.8	0.5	19.6
1419406_a_at	NM_016707	***Bcl11a***	13.8	1.8	7.7
1418271_at	NM_021560	***Bhlhb5***	10.6	1.2	8.8
1452207_at	Y15163	*Cited2*	16.7	2.6	6.4
1449470_at	NM_010053	*Dlx1*	13.8	2.4	5.8
1448877_at	NM_010054	*Dlx2*	9.8	1.8	5.4
1449863_a_at	NM_010056	*Dlx5*	11.2	0.7	16.0
1459211_at	AW546128	*Gli2*	8.0	1.5	5.3
1456067_at	AW546010	*Gli3*	20.6	2.1	9.8
1422851_at	X58380	***Hmga2***	25.5	0.5	51.0
1450723_at	BQ176915	*Ils1*	8.6	0.1	86.0
1427300_at	D49658	*Lhx8*	10.5	0.1	105.0
1417155_at	BC005453	***N-myc***	8.2	1.2	6.8
1415811_at	BB702754	*NP95*	12.6	2.1	6.0
1421193_a_at	NM_016768	*Pbx3*	12.3	1.6	7.7
1417400_at	NM_030690	*Rai14*	11.0	1.6	6.9
1435856_x_at	AV310148	*Smarcb1*	8.0	1.6	5.0
1431255_at	BB656631	***Sox11***	38.7	6.2	6.2
1450034_at	AW214029	*Stat1*	9.6	1.8	5.3
1416711_at	NM_009322	*Tbr1*	9.8	0.2	49.0
1423424_at	BB732077	*Zic3*	11.2	0.5	22.4

Genes reported to participate in cell growth, differentiation and chromatin remodeling are shown in boldface.

Spatio-temporal expression patterns of genes highly expressed in E11.5 NPCs

To substantiate the GeneChip results, we extracted RNA from E11.5 and E14.5 NPCs and performed real-time RT-PCR using specific primers for each selected gene. Consistent with the GeneChip analysis, all five genes were highly expressed in E11.5 NPCs compared with E14.5 NPCs (Fig. 2A). We next performed *in situ* hybridization for each gene using E11.5, E14.5 and E17.5 mouse brain sections (Fig. 2B). *N-myc* and *Hmga2* mRNAs were specifically detected in the ventricular zone (VZ) of E11.5 brain, implying that N-myc and Hmga2 play some role in NPCs at this stage. By contrast, *Bhlhb5*, *Sox11* and *Bcl11a* expression was stronger in cortical plate, where postmitotic neurons reside, than in the VZ (Fig. 2B). We therefore decided to analyze the function of N-myc and Hmga2 in more detail.

Transduction of *N-myc* and *Hmga2* inhibits astrocyte differentiation of E14.5 NPCs

We next examined whether N-myc and Hmga2 affect astrocyte differentiation of NPCs. We expressed EGFP alone (control), and EGFP together with either N-myc or Hmga2, using retroviral infection in E14.5 NPCs, in which expression of the endogenous genes is very low. Virus-infected E14.5 NPCs were cultured for 4 days in the presence of LIF to induce astrocyte differentiation, and then stained with antibodies against GFP and GFAP. As shown in Fig. 3A and B, NPCs infected with control virus effectively differentiated into GFAP-positive astrocytes in response to LIF stimulation (42±2.6%). In contrast, GFAP-positive astrocyte differentiation was virtually abolished in cells ectopically expressing N-myc (0.5±0.4%) and Hmga2 (3±2.0%) (Fig. 3A, B). Expression of these genes did not significantly affect neuronal differentiation of NPCs, as assessed by monitoring expression of the neuronal marker βIII-tubulin, compared with the control cells (Fig. 3C, D). We further examined whether the observed suppression of astrocyte differentiation of NPCs infected with viruses encoding N-myc or Hmga2 could be attributed to specific cell-growth inhibition or to cell death. To address this issue, we performed immune staining for the cycling cell marker Ki67 and the apoptotic marker cleaved caspase 3. Although proliferation of NPCs ectopically expressing N-myc or Hmga2 appeared to be slightly enhanced, expression of either gene caused negligible cell death. These results suggest that N-myc and Hmga2 inhibit astrocyte differentiation of NPCs by a mechanism distinct from that of the neurogenic bHLH factors, which enhance neuronal differentiation (Sun et al., 2001).

Continuous expression of N-myc and Hmga2 in E11.5 NPCs fails to preserve the hypermethylated status of an astrocyte-specific gene promoter

We have previously shown that the *gfap* promoter is highly methylated in E11.5 NPCs, and becomes demethylated as gestation proceeds (Takizawa et al., 2001). This demethylation enables NPCs at later developmental stages, E14.5 or thereafter, to respond to LIF and differentiate into GFAP-positive astrocytes. As shown in the foregoing data, expression levels of *N-myc* and *Hmga2* thus seemed to be reduced concurrently with the developmental stage-dependent demethylation of an astrocyte-specific gene promoter; furthermore, ectopic expression of these genes in E14.5 NPCs inhibited GFAP-positive astrocyte differentiation. We therefore hypothesized that sustained expression of N-myc and Hmga2 in E11.5 NPCs might maintain the hypermethylated status of the *gfap* promoter. To test this, we infected E11.5 NPCs with viruses expressing EGFP alone and EGFP together with either N-myc or Hmga2 and cultured them for 4 days. GFP-positive cells were sorted by FACS and their genomic DNAs were extracted for bisulfite sequencing. As observed in the previous study (Takizawa et al., 2001), the *gfap* promoter including the STAT3 site became demethylated to about 65% in control virus-infected cells after the 4-day culture, and this was also the case for both N-myc- and Hmga2-expressing virus-infected cells (Fig. 3E, F). These results indicate that sustained expression of N-myc and Hmga2 in E11.5 NPCs does not affect the process of demethylation in this astrocyte-specific gene promoter. On the other hand, when 4-day-cultured control virus-infected E11.5 NPCs were then stimulated with LIF for an additional 4 days, GFAP-positive astrocytes appeared, probably due to demethylation in the promoter, whereas neither *N-myc* nor *Hmga2* virus-infected cells gave rise to astrocytes even in the presence of LIF (data not shown). These results suggest that N-myc and Hmga2 inhibit precocious astrocyte differentiation of midgestational NPCs independent of the DNA methylation status of an astrocyte-specific gene promoter.